










An organism-wide atlas of hormonal signaling based on the mouse lemur single-cell transcriptome

Received: 16 August 2022

Accepted: 7 February 2024

Published online: 11 March 2024

 Check for updates

Shixuan Liu ^{1,2,3}, Camille Ezran ^{2,3}, Michael F. Z. Wang⁴, Zhengda Li¹, Kyle Awayan ⁵, The Tabula Microcebus Consortium*, Jonathan Z. Long ^{6,7}, Iwijn De Vlaminck⁴, Sheng Wang ⁸, Jacques Epelbaum⁹, Christin S. Kuo¹⁰, Jérémy Terrien⁹, Mark A. Krasnow ^{2,3}  & James E. Ferrell Jr. ^{1,2} 


Hormones mediate long-range cell communication and play vital roles in physiology, metabolism, and health. Traditionally, endocrinologists have focused on one hormone or organ system at a time. Yet, hormone signaling by its very nature connects cells of different organs and involves crosstalk of different hormones. Here, we leverage the organism-wide single cell transcriptional atlas of a non-human primate, the mouse lemur (*Microcebus murinus*), to systematically map source and target cells for 84 classes of hormones. This work uncovers previously-uncharacterized sites of hormone regulation, and shows that the hormonal signaling network is densely connected, decentralized, and rich in feedback loops. Evolutionary comparisons of hormonal genes and their expression patterns show that mouse lemur better models human hormonal signaling than mouse, at both the genomic and transcriptomic levels, and reveal primate-specific rewiring of hormone-producing/target cells. This work complements the scale and resolution of classical endocrine studies and sheds light on primate hormone regulation.

Hormones are chemical messengers that circulate through the bloodstream and control and coordinate functions of both nearby and distant cells. Since the discovery of the hormone secretin over a hundred years ago¹, about 100 mammalian hormones have been identified². Over the decades, these hormones have been purified, sequenced, and synthesized, their receptors have been identified, and the intracellular signaling pathways they regulate have been explored³. Hormones regulate diverse biological processes ranging from growth and development, reproduction, metabolism, immune responses, to mood and behavior. Many hormones are also therapeutically

significant. For example, the discovery of insulin⁴ changed type I diabetes from an inevitably fatal disease to a manageable one. Likewise, corticosteroids, a class of small-molecule adrenal hormones, are used to treat diverse pathological conditions, including the inflammation attendant to COVID-19, where corticosteroids reduce the death rate in severe cases by ~30%^{5,6}.

The classical endocrine hormones are produced by secretory cells residing in one of the nine endocrine glands. However, it is now clear that other cell types, like fat cells and leukocytes, secrete global regulators into the circulatory system⁷. In addition, some endocrine

¹Department of Chemical and Systems Biology, Stanford University School of Medicine, Stanford, CA, USA. ²Department of Biochemistry, Stanford University School of Medicine, Stanford, CA, USA. ³Howard Hughes Medical Institute, Stanford, CA, USA. ⁴Meinig School of Biomedical Engineering, Cornell University, Ithaca, NY, USA. ⁵Chan Zuckerberg Biohub, San Francisco, CA, USA. ⁶Department of Pathology, Stanford University School of Medicine, Stanford, CA, USA. ⁷Sarafan ChEM-H, Stanford, CA, USA. ⁸Paul G. Allen School of Computer Science & Engineering, University of Washington, Seattle, WA, USA. ⁹Adaptive Mechanisms and Evolution (MECADEV), UMR 7179, National Center for Scientific Research, National Museum of Natural History, Brunoy, France. ¹⁰Department of Pediatrics, Stanford University School of Medicine, Stanford, CA, USA. *A list of authors and their affiliations appears at the end of the paper.

 e-mail: krasnow@stanford.edu; james.ferrell@stanford.edu

functions, like menstrual cycles in human females, depend upon interplay and feedback between multiple hormones and cell types⁸. For these reasons, a complete understanding of endocrine physiology requires comprehensive, global approaches. Variations in hormone regulation and function in different species further complicate the situation. Although comparative studies have shown that many hormones are highly conserved across vertebrates³, the hormone-producing and -receiving cells and their physiological functions are sometimes different⁹.

The gray mouse lemur (*Microcebus murinus*) is a small non-human primate with a lifespan of 5–13 years. Because of its small size, rapid reproduction, and close genetic proximity to humans, the mouse lemur is an appealing model organism for studies of primate biology, behavior, aging, and disease^{10–14}. As described in detail elsewhere^{15,16}, we have recently created, using single-cell RNA sequencing (scRNA-seq), a molecular cell atlas of the mouse lemur by profiling mRNA sequences from ~225,000 cells from 27 mouse lemur organs and tissues from 4 individuals. Given the ethical concerns of primate studies, tissue samples used in the study were collected opportunistically from aged lemurs. Histopathology was assessed for all organs¹⁷; many looked histologically normal, although age- or pathology-related changes were detected in certain tissues such as spontaneous tumors in the uteri of two animals and metastasis in the lung of one^{16,17}. Presumably, the overall hormone network is still operative in these lemurs, but the age of the animals is both a limitation and an opportunity to study disease-associated changes in hormone profiles. Nevertheless, this extensive, organism-wide dataset provides an unprecedented opportunity to study global hormone regulation at single-cell resolution in a non-human primate.

In this study, we present a comprehensive analysis of primate hormone signaling based on the information in the mouse lemur molecular cell atlas¹⁵. We systematically mapped hormone-producing and target cells for 84 hormone classes, and created a browsable atlas that depicts gene expression of hormone ligands, modulators, and receptors. These systematic analyses detected both canonical and unreported sites of hormone secretion and action. We also analyzed the global expression patterns of hormone ligands and receptors, constructed, and characterized an organism-wide cell communication network for hormone signaling, and systematically searched the network for feedback circuits. This analysis revealed a few remarkable principles of hormone signaling and a long list of potential feedback mechanisms. Lastly, we compared hormonal gene expression across humans, lemurs, and mice in selected tissues and cell types, and examined their conservation in expression patterns. This revealed both hormonal genes with a highly conserved expression pattern and ones that show a primate or species-specific expression pattern.

Results

A comprehensive table of genes involved in the biosynthesis and sensing of human and mouse lemur hormones

Although many hormones have been studied for decades, there is not a well-annotated database of hormone ligands, synthases, processing enzymes, and receptors. Therefore, we integrated multiple sources to compile a comprehensive gene table for human hormone signaling (Supplementary Dataset 1). For the hormone list, we mainly referenced the Handbook of Hormones², the “Wikipedia List of human hormones [https://en.wikipedia.org/wiki/List_of_human_hormones]”, and the Handbook of Biologically Active Peptides¹⁸, and added newly discovered hormones including asprosin¹⁹ and the endocrine fibroblast growth factors FGF21, FGF19, and FGF23²⁰. To collect the genes involved in hormone production, we assembled the ligand genes for peptide and protein hormones and the hormone synthesis genes for small-molecule hormones. Maturation or activation of many hormones requires specific enzymes such as angiotensin-converting enzyme (ACE) for angiotensin, the deiodinases DIO1/DIO2 for

thyroid hormones, and prohormone-processing enzymes (e.g., PCSK1, PCSK2, CPE) for many peptide hormones¹⁸. In addition, hormone function may involve endocrine modulators such as IGF-binding proteins (IGFBPs) for IGF1 and specific plasma-binding proteins for most steroid hormones^{21,22}. Accordingly, we added these processing enzymes and modulators for the corresponding hormones. Finally, we curated the hormone receptor genes that are responsible for signaling in the target cells. Most hormones have characterized ligands and receptors, except for endomorphins (tetrapeptides), the ligand gene of which remains unknown. In total, we collected information for 84 groups of hormones and 350 genes, including 102 ligand genes, 41 synthases, 33 processing enzymes/modulators, and 174 receptor genes.

When a hormone included multiple ligand, receptor, synthase, or processing enzyme genes, we incorporated AND/OR logic gates among the genes to determine if a cell type produces or is targeted by a hormone (Supplementary Dataset 1). When two or more of the genes were required for signaling, genes were connected by AND (&) gates. For example, amylin receptors are heterodimeric complexes of CALCR and RAMP proteins, and both subunits are required for function; thus, CALCR and RAMP were connected by an AND symbol. Similarly, AND gates were applied among hormone synthases that catalyze different steps, and between hormone ligands and the corresponding processing enzymes. On the other hand, OR (|) gates were applied when only one of the genes is required for function. For example, there are nine adrenergic receptor genes, all of which function independently and therefore were linked by OR gates.

We next looked up the mouse lemur orthologs of the human hormonal genes in the most up-to-date mouse lemur genome assembly (Mmur_3.0) with both NCBI and Ensembl ortholog databases (Supplementary Dataset 2). Almost all (98.9%, 346/350) of the human hormone-related genes were annotated in the mouse lemur genome, and most (98.0%, 339/346) were one-to-one mappings; seven were many-to-one. The four genes without lemur orthologs (*LHB*, *GALP*, *INSL4*, and *DRD5*) and seven many-to-one mappings could have resulted from incomplete annotation of the mouse lemur genome. For one lemur-unannotated gene *LHB* (luteinizing hormone beta subunit), we identified by sequence homology²³ a candidate *LHB* gene region that has high sequence similarity and the conserved neighboring gene (*RUVL2*) as human *LHB*²⁴ and was selectively expressed in the expected cells (pituitary gonadotrophs) (Supplementary Fig. S1-luteinizing hormone). We concluded that the identified region is likely the mouse lemur *LHB* gene and included it in follow-up analyses. Thus, at least 347/350 (99.1%), and possibly all, of the human hormonal genes are present in the mouse lemur. For comparison, the mouse genome lacks orthologs for six genes (98.3% present, 344/350), five of which are known pseudogenes or have been lost in the mouse genome (*GNRH2*, *MCHR2*, *MLN*, *MLNR*, *NPBWR2* (*Gm14489*)) (Supplementary Dataset 2). In addition, 14 human-mouse orthologs are one-to-many (6), many-to-one (4), or many-to-many (4) mappings, suggesting gene family expansions or contractions in mice or humans. The percentages of human hormonal orthologs present in lemur or mouse genomes were higher than the percentage of all protein-coding genes (PCGs) (>98.9% vs. 89.5% in the mouse lemur genome, and 98.3% vs. 89.8% in the mouse genome). Most (85.8%) human hormone-related proteins were more similar in sequence to their lemur orthologs than to their mouse homologs (Supplementary Fig. S2a). These findings underscore the close similarity between human and lemur hormonal genes.

Organism-wide identification of hormone-producing and target cells

We systematically identified the source and target cells for each hormone by examining the expression of the hormone ligand, synthase, and receptor genes across 739 lemur cell types from 27 different tissues profiled by 10x scRNAseq¹⁵. Source cells were defined as cell types

that expressed above-threshold levels of the ligand (for protein/peptide hormones) or synthase(s) (for small-molecule hormones) plus any necessary modulator genes. Target cells were those that expressed hormone receptor genes. We generated a browsable set of figures and a web portal that depicts the global expression profiles of the hormonal genes (Supplementary Figs. S1 and S3 and Supplementary Dataset 3). Figure 1a–g shows the expression of four representative examples of hormones (in red) and their receptor(s) (in blue) in the identified cell types across the seven, color-coded cell compartments (epithelial, endothelial, stromal, neural, germ, lymphoid and myeloid cells). This analysis identified many canonical sites of hormone secretion and targets, affirming the validity of the single-cell transcriptomic measurements and analysis approach. The analysis also revealed many less-recognized or unreported hormone source/target cells and interesting global patterns of hormone signaling. Below, we highlight a few examples of well-known, lesser-known, and previously unknown sources and target cells. We also showcase examples where hormonal expression is unique in the mouse lemur versus mice or humans.

Prolactin (PRL). Prolactin is a classical endocrine hormone²⁵ secreted by pituitary lactotrophs. In addition to its milk-promoting effect in females, PRL also plays pleiotropic roles in both sexes². These roles include regulation of water and electrolyte balance in the kidney, and control of skin cell proliferation and hair/feather growth and shedding²⁶. Prolactin also plays a major role in energy homeostasis by regulating cell growth and metabolism in the liver, adipose tissues, and pancreas in both sexes²⁷, and may be involved in the immune response²⁸. These sex-non-specific functions are conserved, not just among milk-producing mammals, but across all vertebrates.

As expected, prolactin transcripts were selectively expressed in the lactotrophs of the lemur pituitary gland, and were not detected in other tissues (Fig. 1a–g and Supplementary Fig. S1-prolactin). The prolactin receptor (*PRLR*) message was expressed in both male and female lemurs in the expected cell types, including kidney nephron tubule cells, skin epithelial cells, pancreatic ductal and acinar cells, hepatocytes, intestinal epithelial cells, adipocytes, reticular cells, plasma cells, choroid plexus cells, and the neighboring TSH-secreting thyrotrophs and FSH/LH-secreting gonadotrophs in the pituitary gland (Fig. 1a–g and Supplementary Fig. S1-prolactin). Thus, scRNAseq data confirm that prolactin signaling is similar in mouse lemurs and other animals.

Adiponectin (ADIPOQ) and leptin (LEP). Mouse lemurs undergo dramatic seasonal changes in body weight and fat reserves^{29–31} and therefore may experience seasonally varying levels of adipokines. Adiponectin and leptin are two important metabolic hormones secreted by adipocytes^{32,33}. Although adipocytes were originally regarded only as nutrient storage cells, it is now clear that they also serve an endocrine role³⁴. Surprisingly, leptin transcripts were almost undetectable in the adipocytes captured in the atlas (see discussion in the accompanying manuscript¹⁶) (Supplementary Fig. S1-leptin).

However, adiponectin was abundantly and specifically expressed in mouse lemur adipocytes captured from multiple tissues, including four adipose depots (subcutaneous, mesenteric, interscapular brown, and perigonadal), as well as kidney, limb muscle, pancreas, and bone (Fig. 1a–g and Supplementary Fig. S1-adiponectin). Both *UCPI*-low white-like and *UCPI*-high brown-like adipocytes highly expressed *ADIPOQ*.

Previous research has characterized tissue-specific functions of adiponectin in the liver, pancreas, skeletal muscle, endothelial cells, macrophages, and adipocytes³⁵. While we indeed observed expression of the adiponectin receptor *ADIPOR1* in these tissues in the mouse lemur, we also found *ADIPOR1* to be abundantly expressed in almost all lemur cell types (Fig. 1a–g). Similar ubiquitous expression of *ADIPOR1* has been found in humans and mice (Supplementary Fig. S4). These

results suggest that adiponectin exerts an organism-wide effect through *ADIPOR1*.

In comparison, *ADIPOR2*, the other adiponectin receptor, was expressed more selectively, most notably in the male germ cells and adipocytes (Fig. 1a–g). Interestingly, the lemur expression pattern of *ADIPOR2* differed from that of the human and mouse in which *ADIPOR2* was highly expressed in the liver and only lowly expressed in the testis³⁶ (Supplementary Fig. S4). Alveolar macrophages from the mice, but not humans or lemurs, also showed high *ADIPOR2* expression (Supplementary Fig. S4), suggesting differential *ADIPOR2* effects across the three species.

Motilin (MLN). Motilin is canonically considered a gastrointestinal hormone that is secreted by enteroendocrine cells and regulates gastrointestinal smooth muscle movement¹⁸. However, rodents have lost both the motilin and the motilin receptor genes in evolution³⁷ (Supplementary Dataset 2). The lack of motilin signaling in rodent models has hampered progress on further characterizing motilin function as well as the development of motilin agonists for the treatment of gastroparesis³⁸. Consistent with the canonical view, we observed motilin expression in lemur enteroendocrine cells in the small intestine but not colon (Fig. 1a–g). However, we also observed a broad range of other motilin-expressing cell types, including kidney nephron tubule cells, chemosensory tuft cells from both the airway (lung and trachea) and small intestine, certain brain neurons, adipocytes (higher in *UCPI*-high brown-like adipocytes than in white-like adipocytes), mesothelial cells, and the majority of the *CD4 + CD8-CCL5*-helper T cells (Fig. 1a–g and Supplementary Fig. S1-motilin). The receptor was found to be most highly expressed in pancreatic delta cells and several epithelial cell types of the skin (e.g., sweat gland cells). Together, this expression pattern suggests that motilin is involved in a diverse array of mouse lemur physiological functions in addition to the regulation of gut motility.

Motilin had been detected in the human brain¹⁸, as is the case in the lemur (Fig. 1d), but was not previously known to be expressed in the kidney nephron tubule cells. Therefore, we performed RNAscope, a single molecule mRNA fluorescent in situ hybridization (smFISH) assay to further test whether motilin is expressed in the mouse lemur kidney. This revealed abundant motilin transcripts in the epithelial cells of the proximal tubules but not in the glomerulus, which are mainly composed of podocytes and glomerular capillary cells (Fig. 1h–j). This supports the validity of the scRNAseq results (Fig. 1a–g). It will be interesting to examine, in future studies, motilin expression in other unconventional cell types outside the intestine, explore what functions motilin plays in these cells, and whether their expression is conserved in humans.

Resistin (RETN). Resistin is a phylogenetically recent hormone, present only in mammals². It is expressed mainly by adipocytes in mice but by macrophages, monocytes, and neutrophils in humans^{39,40}. In the mouse lemur, we found that resistin is highly expressed in macrophages, monocytes, and neutrophils, and nearly absent from adipocytes (Fig. 1a–g and Supplementary Fig. S1-resistin), as it is in humans (Supplementary Fig. S4). Interestingly, resistin is also highly expressed in many of the vascular endothelial cell types and in metastatic uterine tumor cells, suggesting additional sources for this hormone in mouse lemurs (Supplementary Fig. S4).

Prohormone-processing enzymes. Prohormone-processing enzymes are required for the maturation of many peptide hormones, including insulin, adrenocorticotrophic hormone (ACTH), gastric inhibitory polypeptide (GIP), and somatostatin¹⁸. The required processing enzymes have been identified for some but not all hormones^{41,42}. In this study, we considered both the ligand and the known or suggested processing enzymes when determining if a cell type produces a

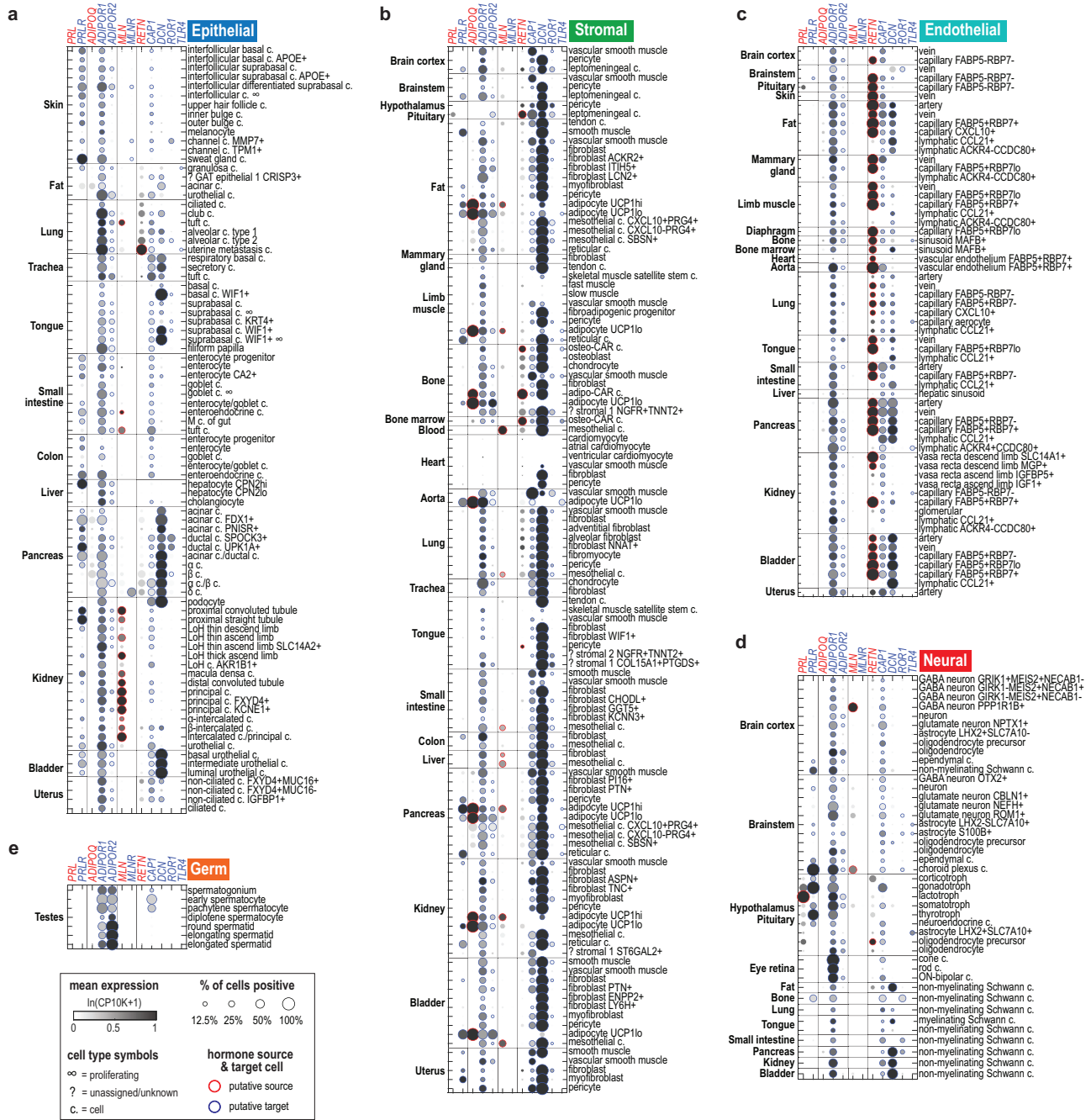


Fig. 1 | Global expression of selected hormone ligands and receptors. a–g Dot plot showing expression of four sets of hormone ligands and receptors across the ~700 mouse lemur cell types, including: prolactin (ligand: *PRL*; receptor: *PRLR*), adiponectin (*ADIPOQ*; *ADIPOP1*, *ADIPOP2*), motilin (*MLN*; *MLNR*), and resistin (*RETN*; *CAP1*, *DCN*, *ROR1*, *TLR4*). Cell types are arranged by compartment: epithelial (a), stromal (b), endothelial (c), neural (d), germ (e), lymphoid (f), and myeloid (g). Rows are cell types, ordered by tissue of origin. Cell-type names are labeled on the right, organs/tissues on the left, and gene symbols on the top (red for ligands, blue for receptors). Dots represent average gene expression (circle color) and percent of cells positive for the gene (circle size). Circle edges indicate above-threshold expression (see Methods) for the ligand (red) or receptor (blue). Potentially low-quality cell types are excluded. Note that granulosa cells and acinar cells, which presumably are derived from the ovary and pancreas, respectively, were also found in perigonadal and mesenteric fat samples, likely caused by accidentally including

small pieces of adjacent tissues during tissue procurement. A complete set of figures that display ligand and receptor gene expression for all 84 hormone classes can be found in Supplementary Fig. S1 and cross-species expression patterns in Supplementary Fig. S4. **h–j** Single-plane confocal images of mouse lemur kidney assayed by RNAscope for precursors of two hormones, motilin (*MLN*) and angiotensin (*AGT*), and the proximal tubule marker cubilin (*CUBN*). Cells were also stained with DAPI to visualize nuclei. Note the *MLN* and *AGT* expression in the *CUBN* + proximal tubule cells and not in the glomerulus, which is mainly composed of podocytes and glomerular capillary cells. Panel **h** shows a global view (merged 20× tile scans) with a single glomerulus in the view and many proximal tubules. The glomerulus and a representative proximal tubule are outlined by dashed curves. **i, j** are magnified views of the boxed areas in (**h**) showing a proximal tubule and glomerulus, respectively. See also Fig. 3b for scRNAseq data on *MLN* and *AGT* expression across kidney nephron epithelium.

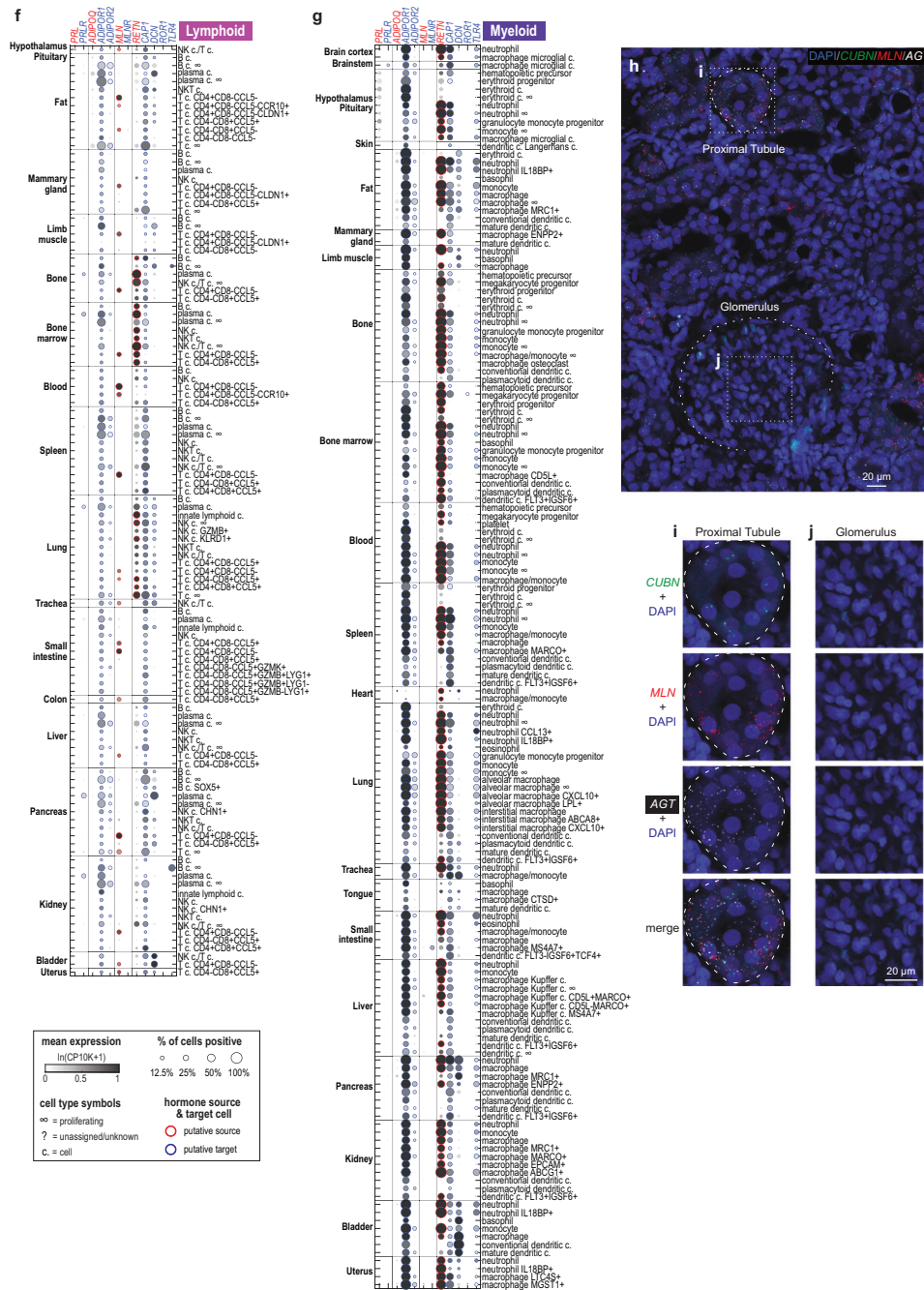


Fig. 1 | Continued

hormone. Selective expression of the processing enzymes can help distinguish hormones that share the same precursor gene. For example, proglucagon (GCG) is the precursor for both glucagon and glucagon-like peptide-1 (GLP-1). *GCG* was expressed in both pancreatic α cells and intestinal enteroendocrine cells, but the two cell types expressed different processing enzymes: α cells expressed only *PCSK2* which is required for glucagon synthesis, and enteroendocrine cells expressed only *PCSK1* which is required for GLP-1 synthesis (Supplementary Fig. S1-glucagon). Thus, as is the case in mice and humans⁴³, α cells are sources of glucagon and enteroendocrine cells are sources of GLP-1 in the mouse lemur.

Interestingly, we noticed that some cell types in the mouse lemur transcribed prohormone genes without expressing the respective processing enzymes. For example, proopiomelanocortin (POMC), which is the precursor of ACTH, melanocyte-stimulating

hormone (MSH), β -endorphin, and lipotropin, is first processed by *PCSK1*⁴⁴. As expected, ACTH-secreting corticotrophs expressed both *POMC* and the necessary processing enzymes, but lemur male germ cells expressed abundant *POMC* without detectable *PCSK1* transcripts (Supplementary Fig. S1-proopiomelanocortin-derived hormones). Similarly, human and mouse male germ cells expressed *POMC* but no *PCSK1* (Supplementary Fig. S4). In addition, lemur male germ cells expressed *GIP*, which also requires *PCSK1* processing; the intestinal and airway tuft cells expressed renin (*REN*) without the necessary *PCSK1* (Supplementary Fig. S1). These results suggest several possible hypotheses: different peptidases are involved, the prohormone transcripts are not translated, the prohormone proteins may function without proteolysis, or the processing enzymes may be expressed below detection levels in the sampled cells.

Plasma-binding proteins. Plasma-binding proteins are not only passive hormone transporters, but can affect hormone functions by modulating hormone half-life and levels of free, active hormones accessible to target cells. Other plasma-binding proteins have been reported to potentiate the binding of hormones to their targets⁴⁵.

Steroid and thyroid hormones are transported in the blood by plasma-binding proteins of the albumin family. While serum albumin (ALB) binds steroids with low specificity and affinity, four other albumins bind these hormones with high specificity and nanomolar affinity, including sex hormone-binding globulin (SHBG) for androgens and estrogens, vitamin-D binding protein (GC) for vitamin D, SERPINA6 for cortisol and progesterone, and SERPINA7 for thyroid hormones^{21,22} (Supplementary Dataset 1). Consistent with the notion that these hormone-binding albumins are produced in the liver^{21,22}, we identified specific expression of *SHBG*, *SERPINA6*, and *SERPINA7* in the lemur hepatocytes, and interestingly higher levels in the *CPN2hi* hepatocytes than in the *CPN2lo* subtype (Supplementary Fig. S1 and see below). *GC* was also expressed in the lemur hepatocytes with a higher level in the *CPN2hi* subtype; however, we also detected notable expression in pancreatic endocrine, ductal, enteroendocrine cells, and cholangiocytes. These sources may contribute to the circulating pool of GC or may have local or exocrine effects, such as regulating intestinal vitamin-D absorption⁴⁶.

In addition, peptide hormones IGF1 and activin are known to be bound by IGF-binding proteins (IGFBPs) and FST, respectively. In contrast to albumins, *IGFBPs* and *FST* were expressed by multiple distinct cell types and showed high cell-type variability (Supplementary Fig. S1).

In summary, we have depicted the organism-wide, single-cell expression patterns for hormones, synthases, hormone modulators, and receptors from 84 classes of hormones, and have systematically identified their sources and targets (Supplementary Fig. S1). This global analysis detected canonical cell types underlying hormone secretion and target functions while also revealing previously unreported source and target cells.

Hormonal gene expression is highly cell-type-specific

Next, we clustered mouse lemur cell types based on the transcriptional profiles of the hormonal genes (Fig. 2a, b). We identified 74 clusters and summarized the hormones and hormone receptors that were expressed by each cluster (Supplementary Dataset 4). We noted that cells of the same type almost always clustered closely irrespective of their tissue of origin, or of the sex or identity of the sampled individual, whereas different cell types were well-separated (Fig. 2b and Supplementary Fig. S5). For example, all lymphatic endothelial cells clustered closely and showed characteristic *IGF1* expression despite their coming from nine different tissues and four individuals (cluster 45, Fig. 3b and Supplementary Fig. S1). Mesothelial cells sampled from eight visceral organs formed a cluster distant from other stromal cells and showed distinctive expression of *NPRI*, *CFB*, *PTGIS*, *ITGB3*, and *PNMT* (cluster 35, Fig. 2b and Supplementary Fig. S1). Although there are only ~300 hormonal genes, ~1% of all detected genes, their expression pattern proved to be indicative of cell-type identity regardless of tissue source or location.

To further test this conclusion, we compared cell-type clustering by either the hormonal genes (~300 genes) or the full transcriptome (>30,000 genes). To visualize the results, we projected the high-dimensional transcriptional data into two-dimensional cell-type maps by uniform manifold approximation and projection (UMAP), which illustrate cell-type similarity based on the selected genes. The cell type UMAPs by either the hormonal genes (~300 genes) (Fig. 2b) or the full transcriptome (Supplementary Fig. S6a) were remarkably similar. The cell-type pairwise distances defined by hormonal genes versus the full transcriptome were also positively correlated, with a Pearson correlation coefficient (r) of 0.70 (Supplementary Fig. S6b). There were

nevertheless minor differences between the two UMAPs. For example, airway and intestinal tuft cells are both chemosensory but are involved in different functions⁴⁷. In the space of hormonal genes, tuft cells from different tissues formed one cluster (cluster 58) with distinctive expression of renin (*REN*), cyclooxygenase 1 (*PTGSI*), arachidonate 5-lipoxygenase-activating protein (*ALOX5AP*, required for leukotriene production), and motilin (*MLN*) (Fig. 2b and Supplementary Fig. S1). However, in the space of all genes, the lung, trachea, and intestinal tuft cells were separated from each other (labeled as 58A*, 58B*, and 58C* in Supplementary Fig. S6). Another notable exception was skin melanocytes, which clustered with oligodendrocytes (cluster 31) when analyzed by only the hormone-related genes (Fig. 2b) but clustered more closely with skin epithelial cell types in the space of all genes (Supplementary Fig. S6a, oligodendrocytes and melanocytes labeled as 31A and 31B, respectively). Thus, cell types were overall similarly clustered by the hormonal genes or the full transcriptomes, and the exceptions showcase rare examples of converged hormonal signaling in distant cell types.

We then assessed how well hormonal gene expression discriminates among different cell types compared to all genes or random sets of PCGs (Fig. 2c–e and Supplementary Fig. S6b–e). As a gold standard, we used the cell annotations described in the accompanying manuscript¹⁵, which are based on the expression of canonical cell markers and iterative clustering with highly variable genes. We then scored how well the cell-type pairwise transcriptional distances for these different sets of genes correlated with a cell annotation-based distance (Supplementary Fig. S7). This annotation-based distance is defined as an integer between 0 and 3: 0 when cell types were annotated with identical names but from different tissues, 1 when the cell annotation names were different but classical histological assignments (Cell Ontology⁴⁸) were identical (i.e., different molecular subtypes), 2 when classical Cell Ontologies were different but cell types were from the same compartment (e.g., both were epithelial), and 3 if cells were different cell types and from different compartments (e.g., endothelial vs. stromal). The pairwise transcriptional distances based on the hormonal genes alone correlated with this annotation-based distance better than that based on the full transcriptome ($r = 0.51$ vs. $r = 0.30$) (Fig. 2c–e). Likewise, the hormonal-based distances correlated better than distances from random sets of PCGs ($r = 0.51$ vs. $r = 0.29 \pm 0.03$, mean \pm SD, $n = 100$) (Fig. 2e). This appeared to be because hormonal genes were more variably expressed across different cell types than average PCGs (Fig. 2f); although the full transcriptome contains more information, the discriminative power is diluted by a large number of low-specificity genes. In support of this idea, when sets of randomly selected PCGs with similar expression variability (dispersion) as hormonal genes were used, the correlation coefficients were similar to that of the hormonal genes (Fig. 2e).

As a further test, we used a continuous Cell Ontology⁴⁸-based metric as the benchmark (Supplementary Fig. S6c–e). This metric was calculated as the mean of the Cell Ontology embedding-based distances from the Cell Ontology graph and the text-based distances from the text descriptions of the Cell Ontology terms⁴⁹. Cell-type distances defined by the Cell Ontology-based metric were positively correlated with those defined by the transcriptional distances of the hormonal genes or all genes, although the coefficient was low (Supplementary Fig. S6c, d). Nevertheless, the hormonal-based cell-type pairwise distances correlated better with this Cell Ontology-based distance than those based on all genes or random sets of PCGs ($r = 0.45$ vs. $r = 0.23$, 0.22 ± 0.04) (Supplementary Fig. S6e), as was the case with the discrete annotation-based distance. Thus, by both measures, hormonal genes do an unusually good job of predicting cell identity.

Finally, we examined if the expression of hormone ligands or receptors alone could distinguish cell types. Interestingly, for most cell-type clusters, hormone ligands or receptors alone classified cell types similarly (Supplementary Fig. S8a–c). This suggests that most

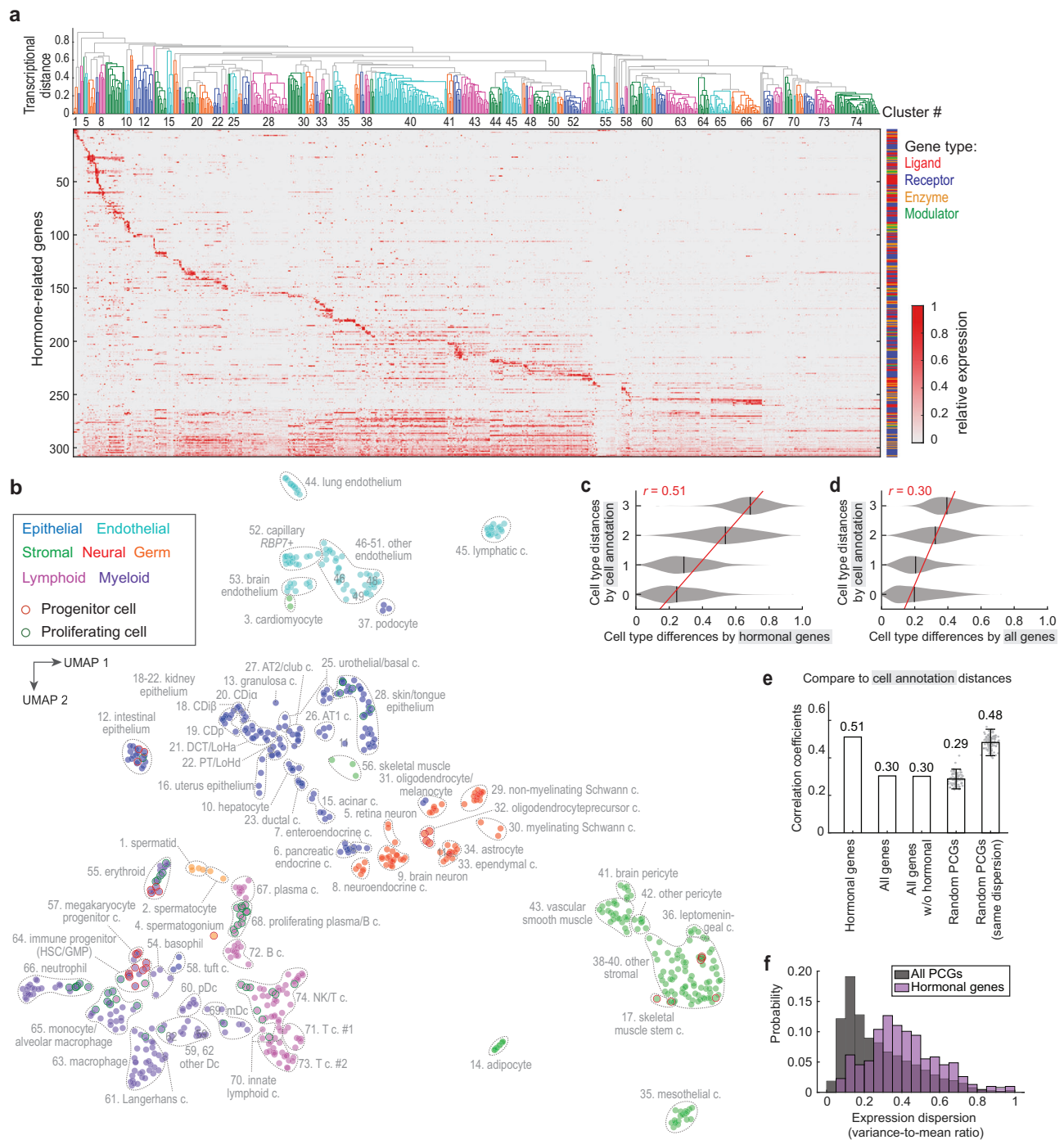


Fig. 2 | Hormonal gene expression is cell-type-specific. **a** Clustering of mouse lemur cell types by hormonal gene expression. At the top is a dendrogram of the hierarchical clustering. Clusters of cell types are color-coded, and cluster numbers are labeled as space allows. The cell types included in each cluster are listed in Supplementary Dataset 4. The lower part of the panel shows a heatmap of relative gene expression levels. Cluster-specific genes are ordered based on the cluster with the highest expression level, with the genes preferentially expressed in the left-hand cell-type clusters on the top. Broadly expressed genes (expressed in more than 35% of cell types) are placed in the bottom and ordered from least to most broadly expressed. **b** UMAP visualization of mouse lemur cell types based on the expression of hormonal genes. Circles are cell types (unique combination of annotation name and tissue of origin) and color-coded by cell-type compartment

types (epithelial, neural, germ, stromal, endothelial, lymphoid, and myeloid). Dashed lines circumscribe the cell-type clusters as in panel **a**, and cluster IDs and names were labeled nearby. One extremely distant cluster (# 35. mesothelial cells) was shifted up in UMAP-2 toward the center of the figure for display purposes. **c**, **d** Hormonal (**c**) or full transcriptome (**d**)-based cell-type pairwise distances compared to the benchmark cell annotation-based distance. r represents Pearson's correlation coefficient. Black vertical lines show distribution means. Red lines show the linear fitting of the data. **e** Correlation coefficients of cell-type transcriptional distances based on different sets of genes with the benchmark cell annotation-based distance. The error bar represents mean and 95% confidence interval of the data ($n = 100$). **f** Distributions of expression variability (dispersion) of the hormonal genes or all protein-coding genes (PCGs).

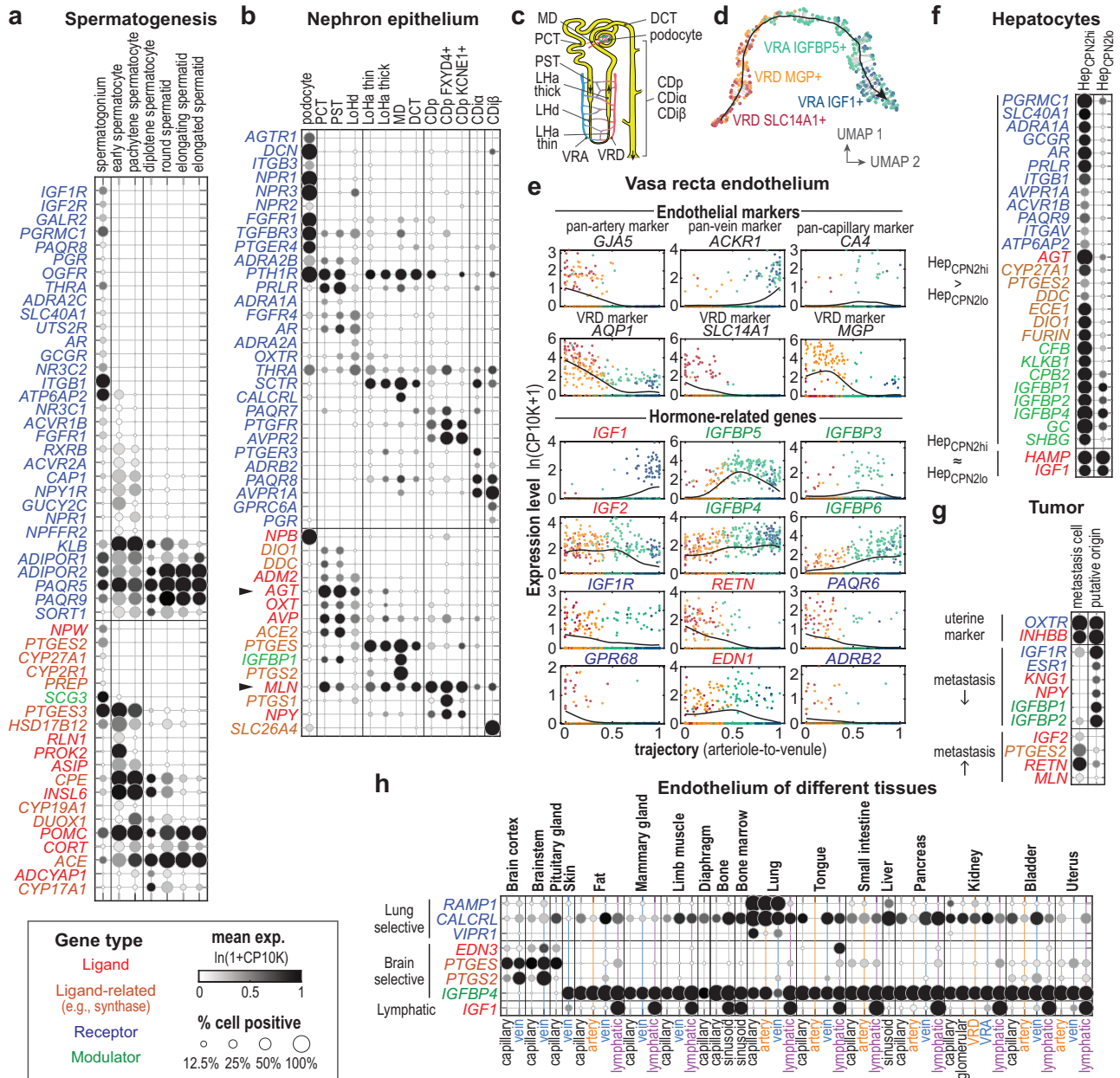


Fig. 3 | Specific hormonal regulation in related cell types. a, b, e–h Dot plots showing expression of hormone ligand, synthase, modulator, and receptor genes that are differentially expressed in **a** male germ cells across different stages of spermatogenesis, **b** epithelial cells along the spatial axis of the kidney nephron tubule, **e** endothelial cells along the arteriole-to-venule spatial axis of the kidney vasa recta, **f** *CPN2hi* vs *CPN2lo* subtypes of hepatocytes, **g** between metastatic tumor cells in the lung (L2) and the putative cell type of metastatic origin (*MUC16*+ non-ciliated uterus epithelial cells, L3), and **h** endothelial cells of the lung and brain compared to other organs. **c** Diagram of the nephron and vasa recta showing the cell types' spatial distribution, related to **(b, d, e)**. **d** UMAP visualization of vasa recta cells based on expression of all genes. The black line shows the detected arteriole-to-venule trajectory with the arrow pointing in the direction of blood flow. Cells are color-coded according to the cell-type annotation names in the atlas. Gray lines show the alignment of the individual cells to the trajectory. In **a**, cell types are arranged along the course of the spermatogenesis. **b** Cell types are arranged according to their spatial distribution along the kidney nephron tubule. Solid arrowheads point to *AGT* and *MLN*; their kidney expression was confirmed by RNAScope (Fig. 1h–j). **h** Endothelial cells are arranged by tissue of origin. **e** Scatter plots show gene expression levels along the arteriole-to-venule trajectory for the endothelial markers and hormone-related genes that are differentially expressed. Shown here is representative data from L4, with similar results in other animals. PCT proximal convoluted tubule, PT proximal tubule, PST proximal straight tubule, LHD loop of Henle thin descending limb, LHa thin loop of Henle thin ascending limb, LHa thick loop of Henle thick ascending limb, DCT distal convoluted tubule, MD macula densa, CDp collecting duct principal cell, CDα collecting duct α intercalated cell, CDβ collecting duct β intercalated cell, VRD vasa recta descending section, VRA vasa recta ascending section.

cell types have stereotypical expression of genes involved in both incoming and outgoing hormonal signaling. A small fraction of clusters were mainly defined by only the ligands or receptors. For example, clusters of pituitary neuroendocrine cells (cluster 7) and tuft cells (cluster 21) were distinguished mainly by hormone ligands, whereas clusters of the skeletal muscle stem cells (cluster 17) and lung

endothelial cells (cluster 51) were mostly based on differences in hormone receptor expression (Supplementary Fig. S8c). In summary, we found that cells generally show stereotypical and cell-type-specific expression of hormone ligands and receptors. Thus, hormone secretion and sensing essentially labels the identity of the cells.

Specific hormonal gene expression in cell subtypes

Hormonal expression could sometimes distinguish cell subtypes that are at different developmental stages, from different locations within an organ, from different organs, or from normal vs. pathological tissue. Below we highlight several such examples (Fig. 3).

Spermatogenesis. Spermatogenesis occurs continuously and asynchronously in the male testis⁵⁰. Thus, sampling the testis at one fixed time point can capture snapshots of the entire process. The atlas includes seven sperm and sperm progenitor cell types that are at different spermatogenesis stages as indicated by the expression of known stage markers¹⁵. The seven cell types fall into three major stages: the undifferentiated spermatogonia, the spermatocytes (which undergo meiosis), and the haploid spermatids that elongate and form mature sperms. Interestingly, these cells exhibited stage-dependent hormone signaling, with over 50 differentially expressed hormone ligands, enzymes, and receptors (Fig. 3a). Previous studies on spermatogenesis have mainly focused on testosterone and on the supporting cells rather than sperms and sperm progenitors^{51,52}. The present data suggest that sperms and sperm progenitor cells are not only differentially regulated by a variety of hormones but may also secrete a changing array of signaling molecules as they mature. The data also clarify some incompletely understood aspects of sperm regulation. For example, progesterone was known to activate a sperm-specific calcium channel prior fertilization to induce Ca^{2+} influx, but the receptor(s) responsible for this effect were unidentified⁵³. The present data show that two non-classical progesterone membrane receptor genes (*PAQR5*, *PAQR9*) are highly expressed in the lemur spermatids and therefore may mediate the process (Fig. 3a). Interestingly, two additional membrane progesterone receptors (*PAQR8*, *PGRMC1*) were specifically expressed in the undifferentiated spermatogonia (Fig. 3a), suggesting that progesterone may also regulate early spermatogenesis⁵⁴. In addition, insulin-like factor 6 (*INSL6*), a member of the secretory relaxin family, was selectively expressed in the lemur spermatocytes (Fig. 3a). Supporting a function in these cells, knockout of *Insl6* arrests spermatogenesis at late meiotic prophase in mice⁵⁵. This analysis suggests that sperms and sperm progenitor cells may directly communicate with other cells via hormones that regulate spermatogenesis and sperm functions. Cross-species comparison among human, lemur, and mouse germ cells identified many of the spermatogonia hormonal genes that exhibited conserved dynamics among all three species, and others showing primate/species-specific expression dynamics (Supplementary Fig. S9a, b, and more discussion below).

Kidney nephron and vasa recta. Although discrete cell types were common in the mouse lemur cell atlas, we noted several cell types that displayed a continuum of gene expression, including the epithelial cells of the nephron and the endothelium of the vasa recta, the blood vessels that supply the renal medulla¹⁵ (Fig. 3d). Interestingly, these cells also displayed gradients of hormone signaling along their spatial axes (Fig. 3b–e).

Nephrons are single-cell layered, one-directional tubules that serve as the structural and functional units of the kidney. We identified a large number of hormonal genes specific to different sections of the nephron epithelium (Fig. 3b, c). Some of these were receptors for hormones known to target specific nephron sections to regulate urine formation. For example, the antidiuretic vasopressin specifically promotes water reabsorption in the collecting duct principal cells², and indeed, the vasopressin receptor gene *AVPR2* was expressed exclusively in the lemur collecting duct principal cells. Interestingly, the collecting duct intercalated cells expressed another vasopressin receptor, *AVPR1A* (Fig. 3b), which has been recently reported to mediate the regulation of acid homeostasis by vasopressin⁵⁶. Although the kidney epithelium is not commonly considered to be an endocrine tissue, many hormone ligands/synthesases were expressed in different

nephron sections, including angiotensinogen (*AGT*), adrenomedullin 2 (*ADM2*), motilin (*MLN*), and neuropeptide Y (*NPY*). Consistent with the scRNAseq results, smFISH by RNAscope confirmed expression of *MLN* and *AGT* in the nephron proximal tubule cells but not in the podocytes and capillary cells of the glomerulus (Fig. 1h–j). Taken together, these data suggest that nephron epithelium may play important roles in hormone production in addition to urine formation.

The vasa recta aligns parallel to the nephron tubules in the kidney medulla (Fig. 3c) and functions collaboratively with the nephrons in urine formation⁵⁷. The vasa recta cells also exhibited a gradual shift in hormonal signaling along its arteriole-to-venule spatial gradient (Fig. 3d). Figure 3e shows the hormonal genes that are significantly differentially expressed along the vasa recta axis. Notably, several genes involved in IGF signaling were differentially expressed: *IGF1*, which was highly expressed in the lemur lymphatic endothelial cells but almost absent from other vascular endothelial types (Supplementary Fig. S1 and Fig. 3h), was highly expressed at the lymphatic-like⁵⁸ venule end of the vasa recta (Fig. 3e); in contrast, *IGF2* and *IGF1R* were more highly expressed in the arteriole end; and four *IGFBPs* (*IGFBP3-6*), which modulate IGF signaling, also exhibited different spatial patterns (Fig. 3e). This spatial organization of IGF signaling may be evolutionarily conserved, as a recent study on mouse kidney vasculature development shows a similar pattern of *IGF1* expression in the mouse vasa recta⁵⁹.

Hepatocyte subtypes. The mouse lemur cell atlas identified multiple previously uncharacterized molecular subtypes of known cell types. For example, the liver hepatocytes of the mouse lemur clustered into two discrete subtypes, the *CPN2hi* and *CPN2lo* hepatocytes. They differed significantly by total transcript count, and may correspond to the small diploid and large polyploid hepatocytes¹⁵. These subtypes were found in both females and males (Supplementary Fig. S10), and seems to be independent of the known zonal heterogeneity¹⁵. Interestingly, a number of hormone-related genes were differentially expressed (Fig. 3f). Hormones including glucagon, androgens, and prolactin appear to selectively target the *CPN2hi* hepatocytes as indicated by differential expression of the corresponding receptors (*GCCR*, *AR*, *PRLR*). In addition, angiotensinogen (*AGT*), precursor for the canonical hepatic hormone angiotensin, was expressed at a much higher level in the *CPN2hi* hepatocytes, whereas no subtype difference was detected in the expression of hepcidin (*HAMP*) or *IGF1*, two other hormones abundantly produced by the liver.

We also identified similar hepatocytes in humans and mice and many of the subtype-specific hormonal expressions were conserved (Supplementary Fig. S9c, d). The hepatocyte subtypes and the subtype-specific hormonal expression were found in both male and female lemurs studied (Supplementary Fig. S10), so are not attributable to sex-specific differences in hormone regulation. However, there may exist other sex-dependent differences in hormone regulation of hepatocytes as observed in other species.

The liver is a central organ of metabolism and plays important roles in hormonal regulation. The detected heterogeneity in hormone signaling suggests potentially important functional divergence between the two subtypes. A deeper understanding of the mechanisms and regulation of hepatocyte hormone heterogeneity would be particularly relevant to the study of mouse lemur-specific physiology, like hibernation/torpor and seasonal body weight changes³⁰.

Metastatic vs. primary tumor cells. The atlas also contains diseased cells, including potential primary endometrial tumor cells in the uterus (*MUC16+* non-ciliated uterus epithelial cells) and lung metastatic cells of endometrial cancer origin, as assessed by tumor gene signatures and histology (see accompanying manuscripts^{15,16}). Both tumor cell types clustered with the non-tumor epithelial cells of the uterus¹⁶ and shared characteristic expression of the oxytocin receptor (*OXTR*) and

the inhibin beta B subunit (*INHBB*) (Fig. 3g and Supplementary Fig. S1), suggesting that the lung metastatic tumor originated from cells resembling the primary *MUC16*+ uterine tumor cells. Certain aspects of hormone signaling seem to have been altered in the metastatic tumor (Fig. 3g). Notably, the tumor cells showed a loss of estrogen receptor (*ESR1*) expression, a change associated with high-grade and advanced-stage endometrial cancers in humans⁶⁰ and more often reported in high mortality type 2 human endometrial cancers⁶¹.

Interestingly, the metastatic tumor cells also acquired new abilities in hormone production. For example, elevated expression of the prostaglandin E2 synthase gene (*PTGES2*) was present in metastatic cells (Fig. 3g). PGE2 has been suggested to be a tumorigenic factor in many cancers⁶². A recent study identified that the PGE2 synthase gene *PTGES2* was elevated in human endometrial cancer tissues and found that PGE2 promotes cell proliferation and invasion in in vitro cell assays⁶³. Resistin was also found to be highly expressed in the metastatic cells (Fig. 3g). Resistin has been reported to promote invasiveness of breast cancer cells in vitro⁶⁴. Thus, endometrial tumors may utilize autocrine resistin signaling to promote metastasis. The shift in hormone signaling identified in the lemur metastatic endometrial tumor is similar overall to that reported in the human. This suggests that the shifts in hormone signaling may be an important step in tumor development and metastasis. Mouse lemurs may serve as a useful animal model to study human cancers that are not well modeled in mice such as endometrial cancers¹⁶.

Vascular endothelium. While hormonal gene expression is generally determined more by cell type than by organ of origin, lung and brain vascular endothelial cells from arteries, veins, and capillaries all exhibited unique organ-specific hormonal signatures (Fig. 3h).

Lung endothelial cells expressed higher levels of mRNAs for the hormone receptors *VIPRI*, *CALCRL*, and *RAMP1* (Fig. 3h) than did endothelial cells from other organs. *VIPRI* is a receptor for vasoactive intestinal peptide (VIP), a strong bronchodilator and one of the most abundant signaling peptides in the lung⁶⁵. Lung-specific *VIPRI* expression was also observed in human but not mouse endothelial cells (Supplementary Fig. S9e, see more discussion below). *RAMP1* forms heterodimeric receptors with *CALCR* or *CALCRL* that are regulated by several hormone ligands including CGRP, adrenomedullin, amylin, and calcitonin, all of which have been reported to have vasodilatory effects². Interestingly, *RAMP1* is expressed in the lung endothelium of the mouse lemur but not in mice or humans, whereas *RAMP2* is expressed in all three species and *RAMP3* is only highly expressed in humans (Supplementary Fig. S9e, see more discussion below). These results suggest that lung vascular endothelium is a unique hormonal target in comparison to vasculature elsewhere, possibly because of the distinctive nature of the pulmonary circulation (e.g., high volume, low pressure) compared to the systemic circulation.

In contrast, brain vascular endothelium was found to express higher levels of a few hormone ligands/synthases. Endothelin-3 (ET-3), a member of the vasoconstricting endothelin family, was selectively expressed in the brain vascular endothelium (Fig. 3h). ET-3 peptide has been detected at various brain locations in rodents, but it remained unsettled what cells secreted the peptide and what physiological role it played⁶⁶. Our results suggest that ET-3 is synthesized by the endothelial cells in the brain, which could target the nearby *EDNRB*-expressing *SLC7A10*+ astrocytes and the *EDNRA*-expressing brain vascular smooth muscle cells and pericytes (Supplementary Fig. S1-endothelin). In addition, the brain endothelium also expressed high levels of *PTGES* and *PTGS2/COX-2* (Fig. 3h), which encode the synthases of prostaglandin E2 (PGE2). PGE2 has been suggested to regulate inflammation-induced fever in mice^{67,68}. Interestingly, brain endothelial cells also selectively lacked expression of *IGFBP4*, which was abundantly expressed in the endothelium of all other tissues in lemurs (Fig. 3h), as in humans and mice (Supplementary Fig. S4).

These organ-specific hormone signatures were expressed at higher levels in endothelial cells than other cell types from the same organ (Supplementary Fig. S1). Thus, it is unlikely that they resulted from cross-contamination (signal spreading). Altogether, lung and brain endothelial cells showcase rare examples of organ-specific (and cell-type-independent) hormonal signaling, which may underlie organ-specific control of the blood flow.

In summary, we have highlighted five examples where closely related cells show detailed specification in their hormone signaling. These examples demonstrate the precise and specialized control of hormonal regulation across different cell types and/or organs.

The hormonal cell communication network is densely connected

Long-range hormonal signaling connects both nearby and distant cells through the bloodstream and enables cross-organ communication. By linking the source cells that produce a hormone ligand to the target cells that express the corresponding receptor, we constructed a global cell communication network for mouse lemur hormone signaling (Fig. 4a). Nodes of the network are cell types, and edges are directed from hormone source to target cells.

The hormone network was remarkably densely connected; 54% of all possible directed edges were found to be present. In fact, in the graphical depiction of the network (Fig. 4a), individual edges are hardly distinguishable because the edges are so dense. The density of the hormone network is comparable to that of the cytokine network⁶⁹, and much higher than the densities of other characterized biological networks (Fig. 4b). For example, the network densities of the yeast, fly, and human protein–protein interaction networks are all estimated to be less than 1%^{70–72}, and the yeast genetic interaction network density is ~3%⁷³. The average degree of a node in the hormonal network was also exceptionally high (Fig. 4c), emphasizing that the average cell communicates with a large number of different cell types. The dense connections between cell types by hormonal regulation are also highly robust: 72% of all existing edges are connected by more than one ligand-receptor pair, and the network maintains high-density connection when randomly removing 10% of the ligand-receptor pairs (Supplementary Fig. S11a).

The hormone network has a high density because most cell types express multiple hormone ligands and receptors (Fig. 4d). On average, cell types expressed 18.3 ± 8.2 (mean \pm SD) receptors or receptor complexes. In comparison, fewer hormone ligands were expressed (2.8 ± 2.6). Only a few cell types expressed 10 or more hormone ligands, and 37.6% of cell types expressed a single ligand or no ligand. This indicates that cells in general respond to more hormones than they produce.

Classical endocrine hormone-producing cells such as enteroendocrine cells, pancreatic endocrine cells, hepatocytes, and neurons were among cells secreting the largest numbers of hormone ligands (Supplementary Fig. S12). Unexpectedly, many stromal cells such as fibroblasts also secreted a large number of ligands, including IGF1, adrenomedullin, angiotensin, and asprosin (Supplementary Figs. S12 and S1). Stromal cells were also particularly rich in the expression of hormone receptors, making them among the most connected cell types in the hormone network (as indicated by their high hubs and betweenness scores, Supplementary Fig. S12). Given the abundance of stromal cells across various tissues, these results suggest stromal cells must play vital roles in endocrine regulation.

Canonically, hormones are believed to be regulated in a hierarchical fashion. Among the most well-known examples are the neuroendocrine cell types of the anterior pituitary—corticotrophs, thyrotrophs, gonadotrophs, lactotrophs, and somatotrophs. These cells are components of regulatory cascades, receiving regulatory signals from one or a few hormones produced in the hypothalamus and in turn producing one or a few hormones to regulate a peripheral

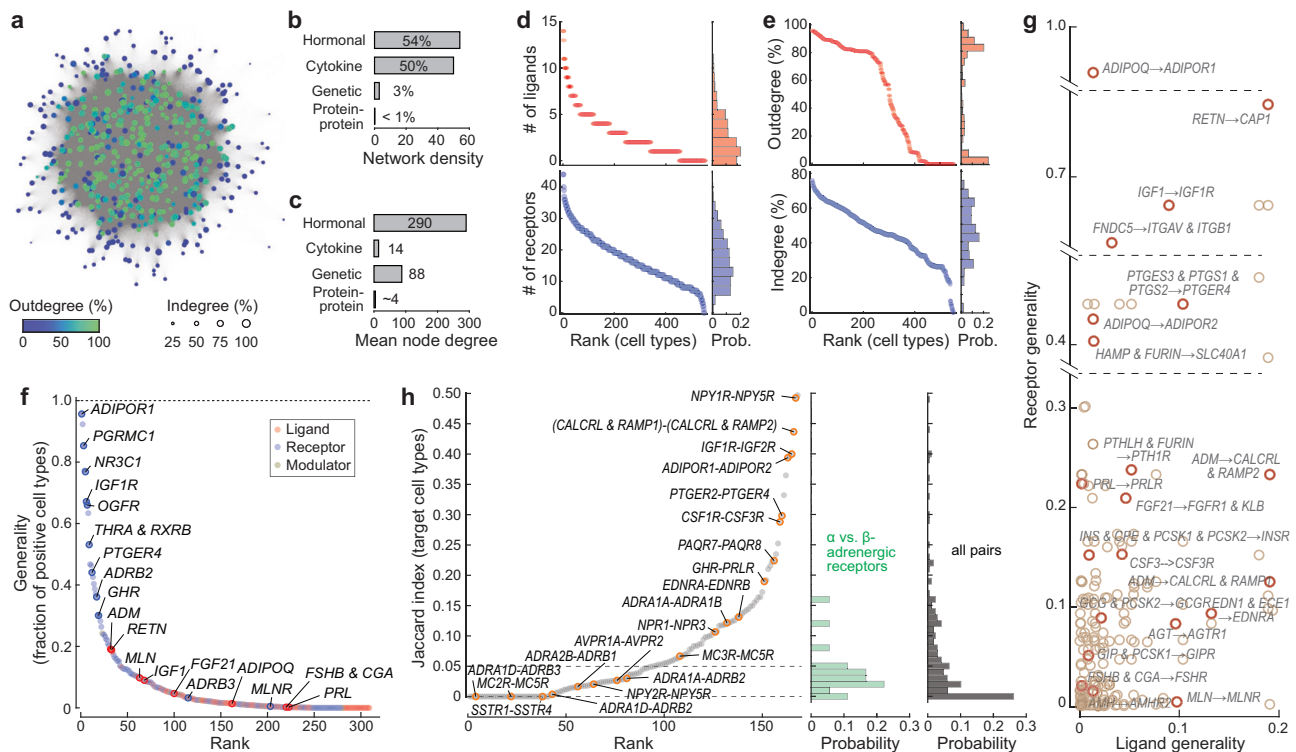


Fig. 4 | The hormonal cell-cell communication network. **a** A representation of the network as constructed by force-directed graph drawing. Nodes (cell types) are color-coded according to the node outdegree (% of cell types connected to the current node by outgoing edges) and the node circle size shows the node indegree (% of cell types connected to the current node by incoming edges). Network edges are directed and connect nodes expressing a hormone ligand to all nodes expressing the corresponding hormone receptor. **b, c** Bar plot of network density (**b**) and average node degree (i.e., the number of connected nodes per node) (**c**) for different biological networks. **d** Number of ligand and receptor types expressed by the network nodes (cell types), ranked from most to fewest. **e** Indegrees and outdegrees of the network nodes (cell types), ranked from high to low values. Node

degree is normalized to the total number of nodes and cluster size and measures the percentage of cell types connected from or to a network node. **f** Generality score of all hormone ligands and receptors ranked from the most generally expressed to most selectively expressed. Generality is defined as the percentage of nodes (cluster size normalized) positively expressing the gene(s) involved in ligand synthesis or receptor binding. Also see Supplementary Fig. S13a for generality score defined as the number of cell-type clusters positively expressing the gene(s). **g** Scatter plot showing generality scores of the hormone ligands and corresponding receptors. Each circle is a unique ligand-receptor pair. **h** Ranking (left) and distribution (right) of Jaccard indices of receptor pairs binding to the same ligand across all hormone receptors.

endocrine gland. Yet these cells were found to express numerous receptors, ranging from 18 (corticotrophs) to 30 (somatotrophs) (Supplementary Dataset 5). These cells appeared to be regulated by growth factors, neuropeptides, neurotransmitters (e.g., dopamine), classical hypothalamic hormones. Likewise, they were found to produce hormones in addition to the classical hormones (Supplementary Dataset 5). For example, corticotrophs expressed the transcripts for galanin (*GAL*), gastrin (*GAS*), and cortistatin (*CORT*), as well as the ACTH precursor *POMC* and its processing enzymes *PCSK1*, *PCSK2*, and *CPE*.

Taken together, this analysis suggests that virtually all cell types across the body are extensively engaged in cell communication via hormonal signaling and that the connections are likely evolutionarily robust to random mutations that disturb hormone regulation. The dense connection of the network results in a large number of highly connected nodes and no obvious network cores (Fig. 4a and Supplementary Fig. S12). This differs from the commonly studied scale-free networks, which are dominated by a small number of highly connected hub nodes⁷⁴. Studies on hormone regulation usually focus on one specific site of secretion and/or target; our analysis emphasizes the importance of a systems view in understanding hormone regulation.

A small number of hormones are global regulators

We next examined the properties of the hormone network edges. In contrast to the protein-protein interaction network and the genetic interaction network, the edges of the hormone communication

network are directional and can be distinguished into different types according to the specific ligand-receptor pairing. The hormone network included 350 different edge types that are selected pairings of 129 ligands and 175 receptors.

Some ligands and receptors were expressed in highly specific cell types, while others were more broadly expressed. We therefore quantified for each ligand or receptor a generality score to evaluate the range of its expression across different cell types in the atlas (Fig. 4f, g, Supplementary Fig. S13a, and Supplementary Dataset 6). Strikingly, a small number of hormone receptors were globally expressed. As mentioned above, the adiponectin receptor 1 gene (*ADIPOR1*) was expressed in 95.7% of the cell types. Other broadly expressed hormone receptor genes included the renin receptor *ATP6AP2* (92.3%), the membrane-associated progesterone receptor *PGRMC1* (85.3%), the cortisol receptor *NR3C1* (76.8%), a putative resistin receptor *CAP1* (77.3%), the IGF1 receptor *IGF1R* (67.1%), the opioid growth factor receptor *OGFR* (66.0%), and the thyroid hormone receptor *THRA* in complex with *RXR*B (53.1%). While it has been recognized that some of these hormones exert organism-wide effects, our results suggest that they target not only a broad range of tissues but likely regulate a large portion or perhaps majority of the cells of the body.

However, the majority of hormone ligands and receptors were expressed in specific cell types; ~85% of the hormone ligands and ~56% of the hormone receptors were detected in less than 5% of the cell types. Certain hormone genes like follicle-stimulating hormone (*FSHB* and *CGA*) were only expressed by a single-cell type. Only a few

hormone ligands were relatively broadly expressed, including adrenomedullin (*ADM*, 19.1%), acylation stimulating protein (*C3*, 19.4%), *IGF2* (18.0%), and resistin (*RETN*, 18.9%). The generality score followed a power-law distribution toward the tail where a small number of globally expressed receptors dominated the distribution (Supplementary Fig. S13b, c). This resulted in a bimodal distribution of the network node outdegree (abundance of outgoing edges/downstream regulation) (Fig. 4a, e and Supplementary Fig. S12). Cells expressing hormone ligand(s) to the high-generality receptors (e.g., adipocytes which secrete adiponectin) sent globally connected outgoing edges, and other cells that only expressed ligand(s) to specific receptors sent a much smaller number of outgoing edges. In contrast, the nodes' indegree (abundance of incoming edges/upstream regulation) was more homogeneously distributed because of the higher specificity of hormone ligand expression and large number of hormone receptors expressed per cell type (Fig. 4d, e and Supplementary Fig. S12).

Alternative receptors for the same hormone tend to be expressed in mutually exclusive cell types

Many hormones can bind to multiple receptors, which may mediate different functions (Supplementary Dataset 1). We therefore examined if receptors for the same ligand tend to be co-expressed or if their expression is mutually exclusive. To quantitatively compare the target cell-type profiles, we calculated a Jaccard index (JI, intersection over union) for each qualifying receptor pair, namely the ratio of cell types that co-expressed both receptors to the cell types that expressed either of the receptors. This analysis revealed that the majority of receptor pairs had low JIs: 24% (41/168) of the receptor pairs had a JI equaling zero, meaning no overlap in their target cell types, and 56% (94/161) had a JI of less than 5% (Fig. 4h). A telling case is the adrenoceptors; although epinephrine (adrenaline) targets many cell types, different adrenoceptor subtypes were selectively employed in different cell types (Fig. 4h and Supplementary Fig. S1-epinephrine/nor-epinephrine). For example, the adrenoceptor genes *ADRA1D* and *ADRB3* shared no target cell types; *ADRA1D* was expressed broadly in vascular smooth muscle cells and pericytes of multiple organs, certain glial cells, and leptomeningeal cells, whereas *ADRB3* mainly targeted adipocytes. Vasopressin receptor genes *AVPR1A* and *AVPR2* also had less than 3% overlap in their target cell types; *AVPR2* was predominantly expressed in the kidney collecting duct principal cells, while *AVPR1A* was highly expressed in the kidney collecting duct intercalated cells and broadly expressed in many stromal cells (Supplementary Fig. S1-vasopressin).

A few receptor pairs showed a tendency toward co-expression, suggesting possible interactions in cell signaling. Supporting this possibility, a top-ranked pair was the IGF receptors *IGF1R* and *IGF2R* (JI = 0.40), which are known to interact in IGF2 signaling. IGF2R internalizes after IGF2 binding and clears IGF2 from the cell surface, and therefore functions as a competitive inhibitor of IGF2-IGF1R signaling^{75,76}. Two other top-ranked pairs were *NPY1R/NPYSR* (receptors for neuropeptide Y, peptide YY and pancreatic polypeptide⁷⁷, JI = 0.49), and *ADIPOR1/ADIPOR2* (receptors for adiponectin, JI = 0.39). Co-expression of *NPY1R* and *NPYSR* has been identified in the rodent brain, and recent studies indicate that the two GPCRs may form heterodimers, resulting in modulated agonist binding properties^{78,79}. Similarly, biochemical studies on ADIPOR1 and ADIPOR2 in cell culture systems suggest that the two receptors can form heterodimers promoting membrane expression of ADIPOR2^{80,81}.

Taken together, this analysis showed that the expression of distinct receptors for the same hormone tends to be mutually exclusive, reflecting functional divergence and specification among hormone receptor subtypes. The rare cases of co-expressed receptors appear to involve functional interaction or cross-regulation between the receptor pairs.

Feedback circuits are widespread in the hormonal cell communication network

Hormone regulation often involves feedback control. We therefore searched the mouse lemur hormonal cell-cell communication network to systematically identify potential feedback regulation. For simplicity, we focused on two-node feedback circuits, namely cell-type pairs that are connected by edges in both directions (Fig. 5a). This systematic search revealed a vast number of feedback circuits; 32% of all node pairs formed feedback circuits, showing that feedback control is widespread in the hormone network (Supplementary Dataset 7). We then tested if feedback circuits are enriched in the hormone network, i.e., more prevalent than would be expected by chance. We applied degree-preserving random rewiring⁸² to randomly permute edge connections without changing node degree (i.e., network edge number and distribution). Figure 5b shows the distribution of the feedback circuit counts from such randomly permuted networks ($n=1000$). Results suggest that feedback circuits are enriched in the hormone network compared to random permutations ($P=0.047$). However, the difference was small (<1% on average). In addition, we randomly removed 10% of ligand-receptor pairs to test how perturbations to ligand-receptor binding affect the feedback distribution of the network. This analysis found that the network feedback circuits remained abundant despite edge removal (Supplementary Fig. S11b) as cell-cell connections usually involved multiple ligand-receptor pairs (Fig. 4d, e). Taken together, this analysis suggests that feedback circuits are abundantly and robustly distributed as a result of the dense connection of the hormone network. Evolution may have further enriched hormonal feedback circuits as suggested by the random rewiring analysis.

We next reviewed selected feedback circuits between endocrine cell types (Fig. 5c–l). The analysis successfully detected well-known feedback regulation. Figure 5c shows the detected feedback loop between pituitary gonadotrophs and the estrogen-producing granulosa cells of the ovary (fortuitously obtained from female perigonadal fat), a classical example of hormonal feedback control that is evolutionarily conserved across vertebrates⁸³. Consistent with humans, lemur gonadotrophs expressed two highly conserved gonadotropins, follicle-stimulating hormone (FSH, a dimer of FSHB and CGA) and luteinizing hormone (LH, LHB/CGA dimer), which target granulosa cells through the corresponding receptors FSHR and LHCGR. Granulosa cells, in turn, expressed key synthases required for the production of sex hormones, which feed back to gonadotrophs through androgen and estrogen receptors (AR, ESRI). Additional feedback regulation from granulosa cells to gonadotrophs was also mediated through anti-Müllerian hormone (AMH) and inhibin/activin signaling. We also detected the well-established feedback loop between pituitary somatotrophs and hepatocytes in the liver, which was mediated through growth hormone (GH), IGF1⁸⁴, and potentially FGF21⁸⁵ and hepcidin signaling (Fig. 5d). In addition, feedback circuits were detected between pancreatic α and β cells through glucagon and insulin signaling and between α and δ cells through glucagon and somatostatin signaling⁸⁶ (Fig. 5e, f).

The analysis also revealed a long list of potential endocrine feedback circuits that have not been reported, or only sparsely reported (Fig. 5g–l). For example, we detected a feedback loop between pancreatic α cells and hepatocytes mediated by glucagon, IGF1 and FGF21 (Fig. 5g). Regulation of hepatocyte glycogenolysis and gluconeogenesis by glucagon is well-established⁸⁷. Less is known about how glucagon affects hepatocyte hormone secretion, and whether the two cell types were involved in feedback regulation. Interestingly, two previous studies have separately shown that injection of glucagon increases plasma FGF21 in humans⁸⁸ and injection of FGF21 reduces glucagon in mice⁸⁹. A recent study also observed that plasma IGF1 and glucagon levels are negatively correlated in non-diabetic humans and found that IGF1 negatively modulates glucagon secretion in an α cell

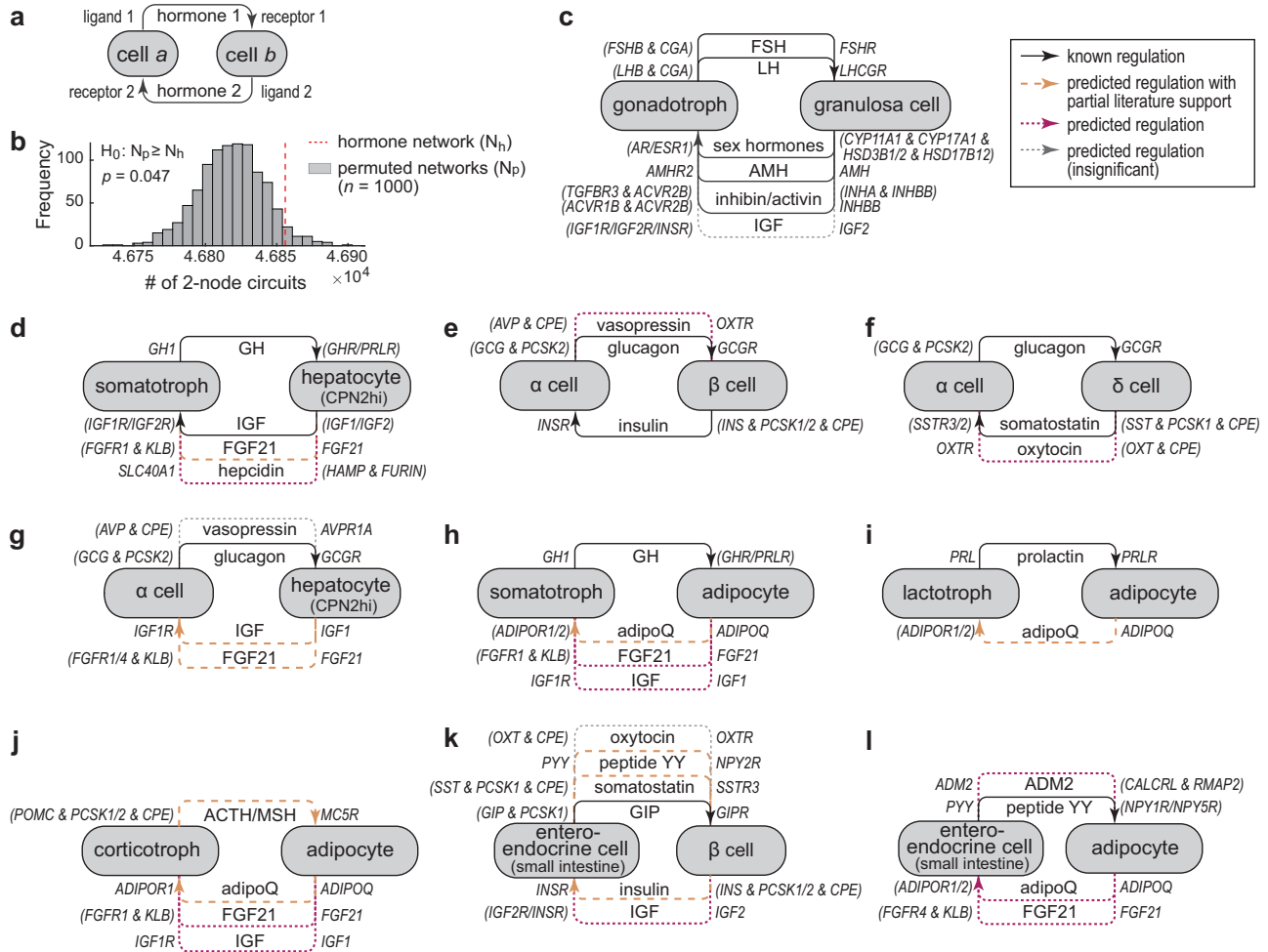


Fig. 5 | Feedback circuits in the hormonal cell-cell communication network. **a** Definition of two-node feedback circuits. **b** Comparison of the number of 2-node feedback circuits identified in the hormonal cell-cell communication network (red dashed line) and that of permuted networks ($n = 1000$), using one-tailed one-sample t -test. Permutation preserved node outdegree and indegree. **c-l** Examples of two-node feedback circuits identified in the network, focusing on the endocrine cell types. Solid black arrows indicate known regulation, dashed orange arrows indicate predicted regulation with partial literature support, and dotted arrows

indicate predicted regulation without earlier knowledge that are potentially biologically relevant (red) or insignificant (gray). A leg is considered biologically insignificant if the connected hormone-producing cell type is unlikely to be the major source of the hormone (cells had lower expression levels than the canonical major source cells) and if the signaling is not local. Parentheses are used to group multiple genes that are expressed in the relevant cell type that function either together (&) or independently (/).

culture model⁹⁰. Considering that the liver is a major source of circulating IGF1 and FGF21, these data suggest that α cells likely form a negative feedback loop with hepatocytes in maintaining metabolic homeostasis.

In addition, adipocytes, through adiponectin, formed possible feedback loops with pituitary neuroendocrine cells, including the growth hormone-secreting somatotrophs, the prolactin-secreting lactotrophs, and the ACTH-secreting corticotrophs (Fig. 5h-j). It has been reported that growth hormone, prolactin, and ACTH reduce adiponectin secretion in adipocytes⁹¹⁻⁹³, but much less is known about the effect of adiponectin on pituitary neuroendocrine cells. Interestingly, a recent study using cultured primary pituitary cells from two non-human primate species found that adiponectin decreases growth hormone and ACTH release and increases prolactin release⁹⁴. Altogether, it suggests that adipocytes form a negative feedback loop with lactotrophs which possibly stabilizes prolactin and adiponectin levels, and form double-negative feedback loops with somatotrophs and corticotrophs, possibly functioning as bistable switches⁹⁵. It remains to be characterized how adiponectin affects pituitary hormone secretion, what are the physiological functions of the pituitary-adipocyte feedback control, and whether this regulation is specific to primates.

Some of the individual legs of the feedback loops shown in Fig. 5 may not be biologically significant. For example, oxytocin and vasopressin are part of the feedback circuits among pancreatic endocrine cells (Fig. 5e, f), between pancreatic α cells and hepatocytes (Fig. 5g), and between enteroendocrine cells and pancreatic β cells (Fig. 5k). The intra-pancreatic feedback regulation (Fig. 5e, f) may be plausible local circuits, but the vasopressin and oxytocin mediated cross-organ communications (Fig. 5g, k) seem less plausible, because most of the oxytocin and vasopressin in the bulk circulation is derived from specific hypothalamic neurons and secreted in the posterior pituitary². The lemur pancreatic endocrine and enteroendocrine cells expressed lower levels of oxytocin and vasopressin than many of the neuronal cell types (Supplementary Fig. S1-oxytocin, vasopressin), thus are unlikely major sources of these hormones in circulation despite their potential role in local communications.

Several others of the regulatory circuits identified here may not fit well with the conventional view, but could nevertheless be biologically significant, such as IGF1- and FGF21-mediated communication from adipocytes to somatotrophs, corticotrophs, and enteroendocrine cells (Fig. 5h, j, l). Canonically, circulating IGF1 and FGF21 are believed to be predominantly produced by hepatocytes^{20,96,97}. However, we identified

high *IGF1* expression in the mouse lemur stromal compartment, in particular adipocytes and fibroblasts (Supplementary Fig. S1-IGF1). *FGF21* expression levels were also comparable between adipocytes and hepatocytes (Supplementary Fig. S1-FGF21). Given that adipocytes are abundant in the mouse lemur and their weight varies by season, it is plausible that adipocytes contribute significantly to the production and temporal variations of the circulating IGF1 and FGF21.

Taken together, this analysis identified an extensive list of potential feedback circuits in the global hormonal cell communication network (Supplementary Dataset 7), providing a rich resource for generating hypotheses on endocrine regulations and to compare their regulatory mechanisms in different species.

Exploring hormonal regulation of the circannual rhythms that control organismal biology

The mouse lemur hormone atlas may bring insights to the study of mouse lemur-specific physiology, such as their circannual rhythms^{31,98}, social interactions⁹⁹, and aging^{12–14,100}. As an adaptation to seasonal environmental changes, mouse lemurs have evolved striking seasonal rhythms in metabolism, behavior, and reproduction that persist throughout their 5–10-year lifespan. Mouse lemurs build fat reserves in preparation for the winter and enter daily torpor, a hypometabolic state, to preserve energy, while in the summer, the animals maintain a lean body and regrow their reproductive organs for mating. The global nature of these phenotypic changes suggests that they may be hormonally mediated. To date, only 12 circulating hormones have been measured in mouse lemurs, but all showed dramatic seasonal changes (Fig. 6a and Supplementary Dataset 8). This suggests that hormones are likely the key messengers coordinating and driving various seasonal changes among different organs. The hormone atlas suggests that these seasonally changing hormones target a broad array of cells and tissues; 95% of the cell types possessed receptors for at least one of these 12 hormones (Fig. 6b–l). Several of the seasonal hormones, such as cortisol, thyroxine, and IGF1 are global regulators, targeting over 50% of the cell types (Fig. 6e–g). Others, such as GLP and GIP, are highly specific, targeting 0.2% and 5% of the cell types, respectively (Fig. 6h, k). Estrogen, androgen, insulin, PYY/PPY target many cell types, but their receptor expression was restricted to only certain cell-type compartments (e.g., stromal, epithelial) (Fig. 6c, d, i, j). For melatonin, receptor expression was not detected (Fig. 6l), possibly due to incomplete sampling of melatonin-expressing brain regions. Comparing across cell types, stromal and epithelial cell types tend to be targeted by most seasonal hormones (Fig. 6c–l). These data suggest that seasonal rhythms engage not only tissues that demonstrate obvious morphological changes (e.g., adipose tissues and gonads), but involve global shifts in cellular metabolism and physiology. While it is now clear that ligands of at least 12 hormones are produced in a seasonal manner in the mouse lemur, it remains to be explored if more hormones are seasonal and if hormone receptors are seasonally expressed to control mouse lemur seasonal rhythms.

Evolution of hormonal gene expression in the human, lemur, and mouse

Lastly, to study the evolution of hormone signaling, we compiled comparable scRNAseq datasets of human and mouse and performed cross-species comparison of hormonal gene expression across human, mouse lemur, and mouse. Six tissues were studied, including lung, skeletal muscle, liver (epithelium only), testis (germ cells only), and two immune tissues, bone marrow and spleen (immune cells only). For consistency, cells from the human and mouse datasets were re-annotated through the same pipeline and with the same cell-type markers as for the mouse lemur cell atlas. Data from different species were further integrated, and cell annotations unified to ensure that cell types are comparable across species¹⁵. This resulted in 62 orthologous cell types with enough cells for comparisons in all three species. We

next identified the hormonal genes with one-to-one-to-one orthology mapping across the three species and examined if the gene exists in all the analyzed scRNAseq datasets (Supplementary Dataset 2). A total of 295 genes were identified and their cross-species expression patterns plotted in Supplementary Fig. S4. By comparing the correlation of the overall hormonal gene expression, we found that human and lemur showed a higher (P value = 0.006) correlation coefficient ($r = 0.50$) compared to that between human and mouse ($r = 0.48$) (Fig. 7a), suggesting that overall hormonal gene expression is more similar between humans and lemurs compared to mice. For comparison, the mean sequence identity between these 295 human and lemur one-to-one orthologs was 0.86, and for human and mouse orthologs 0.82 (Supplementary Fig. S2b). Thus, humans are more similar to lemurs in both gene sequences and expression patterns, than they are to mice.

Next, we examined individual hormonal genes and compared the conservation of their expression patterns between the orthologous cell types of human and lemur vs. that between human and mouse. For each gene, we calculated the correlation coefficient for expression in the 62 orthologous cell types for human vs. lemur (i.e., $r(\text{human, lemur})$), human vs. mouse ($r(\text{human, mouse})$), and lemur vs. mouse ($r(\text{lemur, mouse})$), and we used the correlation coefficients as a gauge of expression pattern similarity (Fig. 7b, c). Many of the genes showed a conserved expression among all three species, such as endothelium-specific *RAMP2*, liver-specific *GC*, and fibroblast- and pericyte-specific *EDNRA* (Fig. 7b–d and Supplementary Fig. S4).

Interestingly, four genes (*RETN*, *VIPRI*, *PROK2*, and *PTGDR*) were highly correlated between human and lemur but poorly correlated between human and mouse (Fig. 7b, c), suggesting that their expression patterns are conserved in primates and/or diverged in mice. As discussed above, *VIPRI* (vasoactive intestinal peptide receptor 1) was selectively expressed in the lung endothelial cells of humans and lemurs but not mice (Fig. 7d and Supplementary Fig. S9e). *RETN* (resistin) was most highly expressed in the neutrophils, monocytes, and macrophages in humans and lemurs but not mice (Fig. 7d). Similarly, *PTGDR* (prostaglandin D2 receptor) was expressed in the natural killer (NK) and NK T cells in humans and lemurs but not mice (Fig. 7d). *PROK2* (prokineticin 2) was selectively expressed in neutrophils and at lower levels in other myeloid cells in humans and lemurs, but was not expressed in these cell types in mice; instead it was expressed in spermatocytes (Fig. 7d).

In contrast, only one gene, neurotensin (*NTS*) was found to be more similar between human and mouse versus that of human and lemur, when applying the same threshold (Fig. 7b, c). Among the cell types examined in all three species, *NTS* was selectively expressed in the lymphatic cells in human and mouse but not lemur (Fig. 7d). Across all mouse lemur atlas cell types, *NTS* was most highly expressed in the small intestine enteroendocrine cells (Supplementary Fig. S1-neurotensin/neurotensin N), which is also the canonical site of *NTS* secretion in humans¹⁸. However, we currently lack cross-species scRNAseq data of the enteroendocrine cells for comparison. Presumably, the major site of *NTS* secretion is conserved across the three species (in enteroendocrine cells), whereas the uncanonical lymphatic *NTS* expression is specific in humans and mice but not lemurs. It will be interesting to compare, in human and mouse, levels of *NTS* expression in the lymphatic cells to that of enteroendocrine cells and explore the function of this uncanonical source of *NTS*.

We also identified one gene (*PAQR5*, which encodes a membrane progesterone receptor) whose expression pattern is more similar between lemur and mouse than between either of the species and human (Fig. 7c). Both lemur and mouse spermatids show the highest *PAQR5* expression, whereas human cholangiocytes show the highest expression among the cell types examined (Fig. 7d).

In addition, a number of genes showed low conservation in their expression patterns among all three species, such as *RAMP1*, *RAMP3*,

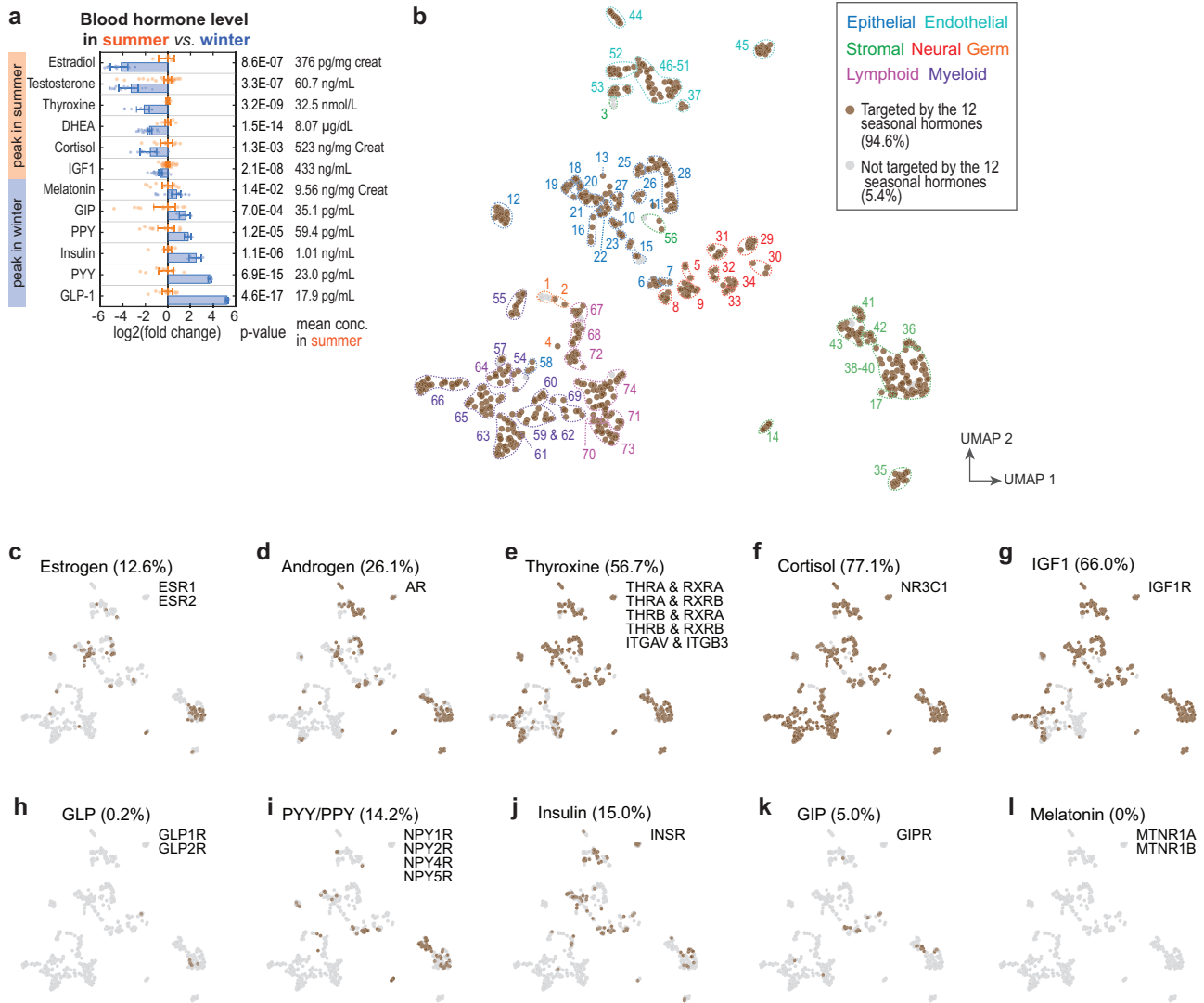


Fig. 6 | Seasonality of hormone concentrations in the mouse lemur affects almost all cells and tissues. **a** Concentrations of twelve hormones measured under long-photoperiod (daily 14:10 h light:dark, summer-like) and short-photoperiod (10:14 h light:dark, winter-like) conditions in captive mouse lemurs. Animals were kept indoors under constant temperature (24 °C) and with photoperiods alternated between long and short photoperiods every 6 months. Bars represent fold changes in hormone concentration compared to average summer levels. Error bar represents mean and 95% confidence interval of the mean. *P* values were calculated by two-sided two-sample *t*-tests comparing summer versus winter concentrations. Data are listed in Supplementary Dataset 8, collected from literature as follows and supplemented with additional measurements: estradiol^{137,138}

(*n* = 5 for summer, 11 for winter), testosterone^{139–141} (*n* = 28, 15), thyroxine^{137,142} (and additional data in Supplementary Dataset 8, *n* = 6, 10), DHEA¹³⁸ (*n* = 14, 30), cortisol¹⁴³ (and additional data in Supplementary Dataset 8, *n* = 12, 12), IGF1¹⁴⁴ (*n* = 33, 37), melatonin¹⁴⁵ (*n* = 15, 19), and gut hormones^{146,147} GIP (*n* = 12, 16), PYY (*n* = 12, 5), insulin (*n* = 11, 6), PYY (*n* = 12, 6), and GLP-1 (*n* = 12, 6). **b** Mouse lemur cell types targeted by any of these 12 seasonal hormones. Cell types are displayed in the same UMAP plot as in Fig. 2b. Circles are cell types and are color-coded according to whether they express receptors for any of the 12 hormones. Dashed lines circumscribe the cell-type clusters and are colored according to cell-type compartments. **c–l** Mouse lemur cell types targeted by each of these 12 seasonal hormones displayed in the same UMAP format as in (b).

PTGDS, *PNMT*, *PAQR6* (Fig. 7b–d). For example, *RAMP1*, as previously discussed, was most highly expressed in the lung vascular endothelial cells in the lemur. However, mouse myeloid cells, such as monocytes, macrophages, and dendritic cells show the highest *RAMP1* expression. In humans, *RAMP1* was moderately expressed in the lung ciliated epithelium, hepatocytes (*CPN2hi* subtype), and skeletal muscle cells, two of which also displayed moderate *RAMP1* expression in the lemur and mouse.

Lastly, the cross-species dataset included male germ cells which form a continuous gradient of expression patterns (Fig. 7e, f). Spermatogenesis is known to have undergone extensive molecular evolution¹⁰¹. Thus, we analyzed the expression dynamics of the stage-specific hormonal genes identified in Fig. 3a and examined their conservation across the three species (Fig. 7g, h and Supplementary

Fig. S9a, b). Although many spermatogonia-specific hormonal genes showed a conserved expression across the three species, some genes displayed species differences. Some involve small shifts or modifications in the expression dynamics. For example, consistent across all three species, *PTGES3* expressed in spermatogonia and spermatocytes and not in spermatids (Fig. 7g, h). However, in humans and lemurs, *PTGES3* expression was gradually reduced in the course of sperm differentiation, whereas in mice expression was maintained at a high level through mid to late spermatocytes (Fig. 7g, h). Other species-specific expression involved lack of expression, or substantially reduced expression. Examples include the previously discussed *PAQR5*, which was highly expressed in spermatids in lemurs and mice, but only slightly expressed in human spermatids. In addition, *PGRMC1* was expressed only in spermatogonia in humans and lemurs, and was

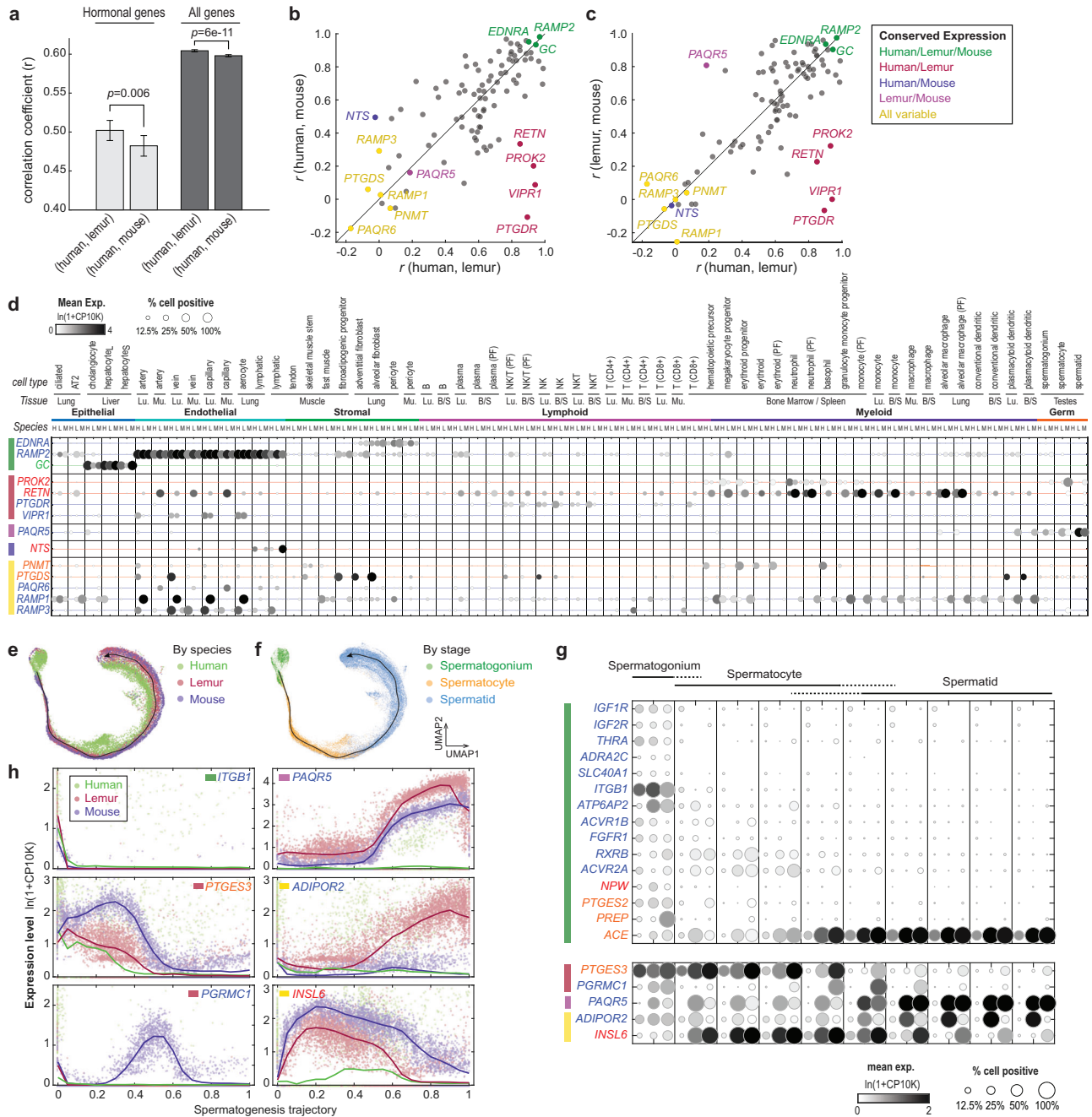


Fig. 7 | Cross-species comparisons of hormonal gene expression across humans, mouse lemurs, and mice. **a** Correlation coefficients of overall expression patterns for all the hormonal one-to-one orthologs (left) or all one-to-one orthologs (right) between human and lemur vs. between human and mouse. Error bars show 95% confidence intervals. p value indicates the significance of a higher correlation between human and lemur vs. between human and mouse, calculated by comparing the two correlation coefficients with one-tailed test after Fisher’s Z-transformation. Sample sizes for the calculation of correlation coefficient are 18,290 (295 genes * 62 cell types, left) and 831,234 (13407 * 62, right), respectively. **b** Comparison of correlation coefficients between the expression patterns of human and lemur (x axis) versus that between human and mouse (y axis) for individual hormonal genes. **c** Comparison of correlation coefficients between the expression patterns of human and lemur (x axis) versus between lemur and mouse (y axis) for individual hormonal genes. Black lines in (b, c) indicate 1-1 relationship between the two coefficients. **d** Dot plot showing expression patterns of highly species-conserved and species-variable example genes in the 62 orthologous cell

types across all three species. Rows are orthologous genes, indicated with the respective human gene symbols. Columns are cell types, displayed as triplets of the respective expression in humans, lemurs, and mice. Vertical gray lines segment different cell-type triplets. Cell types are ordered first by compartments, then by tissue, and finally by species. **e, f** Species-integrated UMAPs of the male germ cells with cells color-coded by species (**e**) or spermatogenesis stage (**f**). Black lines indicate the identified spermatogenesis trajectory with arrows pointing to the direction of maturation. **g** Dot plot showing cross-species expression patterns of spermatogenesis stage-specific hormonal genes in germ cells grouped and ordered by the integrated spermatogenesis trajectory. Cell grouping in the UMAP format is shown in Supplementary Fig. S9a. **e** Scatter plots showing the species-conserved or species-variable expression patterns of example genes in (**g**). Points are single cells color-coded by species. Solid curves show a moving average of the expression level along the spermatogenesis trajectory. **d, g, h** Colored bars next to the genes indicate the species conservation patterns as in (**b, c**).

highly expressed during the spermatocyte-spermatid transition in mice (Fig. 7g, h).

Taken together, cross-species comparison revealed an overall more similar pattern of hormonal gene expression between human and lemur vs. human and mouse. Analysis of individual hormonal genes identified interesting examples that are highly conserved or display primate/species-specific expression. This analysis revealed interesting candidates for future studies to understand the evolution of individual and global hormone signaling.

Discussion

Hormonal signaling is vital to multicellular life, allowing cells to communicate with both surrounding cells and remote cells in other tissues. In this study, we systematically mapped hormone-producing and -target cells across the 739 cell types from 27 different tissues from the mouse lemur molecular cell atlas. We generated a browsable atlas that depicts gene expression of ligands, modulators, and receptors for 84 hormone classes (Supplementary Fig. S1). This dataset complements the scale and resolution of classical endocrine studies and brings a cellular and molecular foundation for studying primate hormone regulation.

The hormone atlas also provides an opportunity to extract global principles of hormone signaling. The hormone-related genes exhibited cell-type-dependent, stereotypical expression patterns, and their transcriptional profiles faithfully define cell-type identities, despite their constituting less than 1% of the transcriptome (Fig. 2). Ligands or receptors alone also classified cell types well, with certain clusters mostly defined by their ligands and others by their receptors (Supplementary Fig. S8). Cell-type clusters defined by the hormonal genes often show further cell type, subtype, or stage-dependent specification within clusters, such as the extensive shifts in hormonal signaling during spermatogenesis, across the spatial gradient of the kidney nephron epithelium and vasa recta endothelial, between subtypes of hepatocytes, and during tumor metastasis (Fig. 3a–g). There is also an interesting organ-dependent clustering of the lung and brain vascular endothelial cells, showcasing a rare example of organ-specific rather than cell-type-specific hormone signatures (Fig. 3h). Altogether, it is remarkable how well a cell's intercellular communication repertoire encapsulates the cell's identity, indicating precise and highly specialized hormonal control in different cells across the body.

To study the properties of global hormonal regulation, we constructed an organism-wide cell communication network for mouse lemur hormone signaling, by connecting the hormone-producing cells to the corresponding target cells (Fig. 4). This hormone network was exceptionally dense (Fig. 4a, b), which mainly resulted from two network features. First, most cells in the network expressed multiple hormone receptors and/or ligands (Fig. 4d). Second, although most hormone ligands and receptors were expressed in specific cell types, a small fraction of hormone receptors were nearly ubiquitously expressed, resulting in almost global connection of the relevant hormone-producing cells (Fig. 4e–g). Thanks to its dense connection, the hormone network is highly robust to random perturbations that delete individual edges (Supplementary Fig. S11). Although the regulatory circuits of individual hormones may be hierarchical, as classically viewed, overall the network is decentralized, which de-emphasizes the contribution of any one hormone receptor pair. Many of the hormone-secreting cells are diffusely distributed throughout the organism, in line with the concept of a diffuse neuroendocrine system espoused by Feyrter¹⁰². It is worth noting that, although changes to a single hormone receptor pair may only minimally affect the overall hormone network structure, the impact to animal physiology and metabolism could be significant. Information flow in the hormone network depends not only on whether an edge exists but also the identity of the connecting edge(s), i.e., the hormone receptor pair(s). Interestingly, despite the density of the hormone

signaling network, subtypes of hormone receptors that bind to the same ligand were generally expressed in a mutually exclusive fashion, supporting the notion that different hormone receptor subtypes usually mediate different physiological functions through separate target cells (Fig. 4h).

Feedback regulation was widespread in hormonal signaling, and it was robust to network perturbations (Fig. 5b and Supplementary Fig. S11b). The analysis identified well-known feedback circuits among several endocrine cell pairs and detected additional, previously unreported, hormones involved in feedback control (Fig. 5c–f). We also identified many previously unreported feedback circuits (Fig. 5g–l and Supplementary Dataset 7) which may be involved in adaptation or homeostasis (negative feedback circuits) or in generating switch-like responses (positive and double-negative feedback circuits). It is worth emphasizing that not all detected feedback circuits will necessarily be biologically significant. In particular, for hormones that travel and mix in the bulk circulation for long-distance cell communication, signals from a particular hormone-producing cell type could be overwhelmed by other cell types that produce larger amounts of the same hormone. Future analysis may include information on cell numbers of individual cell types and genes responsible for rate-limiting steps to more systematically compare total hormone production in each cell type and discriminate major and minor hormone sources. Nevertheless, this analysis represents an initial step to systematically identify endocrine feedback circuits for future functional validation and characterization. Our findings may also inform studies of the systems biology and network topology of hormone signaling (see for example, ref. 103).

Mouse lemurs display dramatic seasonal changes in body weight, hibernation propensity, and reproductive activities^{31,98,104}. Such seasonal rhythms are likely regulated, at least in part, by seasonally varying long-range hormones that coordinate the changes across different organs of the body (Fig. 6a). The hormone atlas shows that almost all (95%) of the mouse lemur cell types are regulated by seasonally varying hormones (Fig. 6b). This suggests that most, if not all, mouse lemur cells across all organs of the body experience seasonal changes in metabolism, growth, and function. By systematic mapping of hormone-secreting and target cells, the atlas also points to candidate cell types and signaling to explore the upstream and downstream regulation for each of the seasonally varying hormones. Given that all 12 hormones measured in the mouse lemur showed significant seasonal changes, we suspect that more hormones will prove to be seasonal. Future work should systematically characterize seasonal patterns of hormones with higher temporal resolution, and to sample animals in different seasons to detect seasonal expression changes in hormone receptors, ligands, and synthases, which could indicate seasonal restructuring of the hormone network. Circannual rhythms are widespread in nature^{105,106} and humans display seasonally varying hormone levels and cellular transcriptomes^{107–109}. The findings of the present study may apply to species beyond the mouse lemur, and may provide insight into season-associated human diseases^{110–112}.

Mouse lemurs are genetically closer to humans than mice are. Likewise, the lemur better models human hormonal signaling than does the mouse. At the genomic level, there were fewer hormonal genes that were lost (or became pseudogenes) in lemurs (3) than mice (6). More human genes had one-to-one mapping in lemur (338, if counting *LHB*) than mouse (330). Further, more human genes (85.8%) had a higher sequence identity with their lemur ortholog than their mouse ortholog (Supplementary Fig. S2). Given that mouse lemur genome and gene annotations remain lower in quality than those of humans and mice, some of the lemur genes may be unannotated or incorrectly annotated, like *LHB*. Thus, the above comparisons may underestimate human-lemur similarity. Lastly, by comparing the expression patterns of the one-to-one orthologs across the three species, we also found mouse lemurs had an overall higher similarity with humans compared to mice (Fig. 7a). For hormonal genes that

show a highly species-specific expression pattern, more (4) were conserved between humans and lemurs and unique in mice compared to the opposite (only 1) (Fig. 7b).

Single-cell RNA sequencing is a powerful tool for assaying cellular function and activity, but there are limitations. Although the technique has improved rapidly in sensitivity, accuracy, and efficiency, scRNAseq still faces low capture efficiency and high transcript dropout¹¹³. With the large number of cells assayed in the mouse lemur molecular cell atlas, we averaged gene expression across cells of the same cell type to smooth the noise in individual cells from dropout. In the analysis of hormone regulation, genes involved in hormone production, such as ligands and modulators, tended to be abundantly expressed; but certain hormone receptor proteins may be low in copy number and slow in turnover, and therefore may result in false-negative errors. In addition, there can be false-positive errors caused by contamination from other cells in the same sample (i.e., signal spreading). This is most notable for abundantly expressed ligand genes and tissues affected by endogenous digestive enzymes (e.g., pancreas). In this study, we scored positive expression of a hormone ligand only when both the ligand gene and the necessary modulators (such as prohormone-processing enzymes) were present. This approach mitigated false-positive detection of highly abundant ligands. Lastly, scRNAseq has low capture efficiency for certain cells such as neurons and large-sized adipocytes. Particularly relevant for the study, hypothalamic neurons were not captured in the current lemur dataset. Nevertheless, the mouse lemur cell atlas included several neuronal subtypes from the brain cortex, brainstem, and retina, as well as both *UCPI*-high and *UCPI*-low adipocytes from multiple tissues¹⁵. Although not yet a complete nor ideal sampling, the mouse lemur cell atlas is one of the most comprehensive and accurately annotated organism-wide scRNAseq datasets reported to date. Other organism-wide scRNAseq atlases have been created or are being created for other species, including mouse^{114–116}, ascidian¹¹⁷, macaques^{118,119}, and human¹²⁰, bringing exciting resources to the study of the evolution of hormone signaling.

Finally, it is worth emphasizing that the mouse lemur scRNAseq atlas used in the study was constructed with four aged and diseased donors. For example, both females had uterine tumors with metastasis, and all four lemurs exhibited chronic kidney disease which may have affected the transcriptional profiles of the kidney cells. Nonetheless, in the cross-species analysis, we have shown that hormone profiles of individual cell types are overall conserved across human, lemur, and mouse. Human and lemur actually correlated better in their overall transcriptional and hormonal profiles than between human and mouse, despite the fact that mouse data were derived from younger, healthier animals¹¹⁴ and that human data was possibly affected by different pathologies¹²⁰. While previous studies reported that concentrations of hormones may change over age¹²¹, we suspect that the global principles of hormone signaling—e.g., a densely connected, decentralized network with abundant feedback regulation—learned through the mouse lemur atlas may also be pertinent to younger lemurs and likely apply to other species. In addition, we have taken advantage of the disease conditions of the mouse lemurs, such as the two females with primary and metastatic uterine adenocarcinoma, which revealed interesting metastasis-associated changes in hormone profiles.

Traditionally, biologists focus on one particular cell type and/or organ system. However, hormone signaling by its very nature connects different cell types and organs. The emerging organism-wide atlases open a door in understanding the cross-organ communication systems that allow organisms to function as a reliable robust whole.

Methods

Animals husbandry, tissue procurement, and processing

Details on animal husbandry and sample collection and processing have been described in accompanying manuscripts^{15,17}. In brief, mouse lemurs (*Microcebus murinus*) were maintained for noninvasive

phenotyping and genetic research as approved by the Stanford University Administrative Panel on Laboratory Animal Care (APLAC #27439) and in accordance with the *Guide for the Care and Use of Laboratory Animals*¹²². Animals were housed indoors in an AAALAC-accredited facility in a temperature (24°C) and light-controlled environment (daily 14:10 h and 10:14 h light:dark alternating every 6 months to stimulate seasonal breeding behavior and metabolic changes). Animals ($n = 4$) in declining health that did not respond to standard therapy were euthanized by pentobarbital overdose under isoflurane and tissue samples were collected for scRNAseq and histopathology analysis. Euthanasia took place during summer-like long-photoperiod season for all lemurs. Age and sex of the individuals were as follows: L1, male, 9.8 y; L2, female, 10.1 y; L3, female, 11.8 y; L4, male, 11.8 y. Details of animal histopathology can be found in Casey et al¹⁷ and tissue sampling/processing pipelines has been described in the accompanying manuscript¹⁵. Pathologies common to all four animals were fibrous osteodystrophy, chronic renal disease, uterine tumors (females only), cataracts, and osteoarthritis. Tissues not described in ref. 17 were histologically normal.

RNAscope experiments

Mouse lemur-specific RNAscope® probes for *MLN*, *AGT*, and *CUBN* were designed and produced by Advanced Cell Diagnostics, Inc. (ACD) (cat #. 1260231, 1263051, 1263061). The kidney samples analyzed were collected from one of the lemurs (L4) profiled by scRNAseq¹⁵ and analyzed in this study. Samples were procured, fixed, dehydrated, OCT-embedded, and biobanked at -80°C . Cryosections (15- μm thick coronal sections) of the kidney were prepared using a Leica Cm3050s cryostat, stored overnight at -80°C , and subsequently processed using the standard RNAscope multiplex fluorescent v2 protocol for fixed-frozen samples (UM 323100 Rev B), with the RNAscope® Multiplex Fluorescent Reagent Kit v2 (cat#. 323270). In brief, two sections were first pre-treated during which tissue slides were PBS washed, baked, post-fixed, dehydrated by ethanol, treated with hydrogen peroxide, submerged in RNAscope 1X Target Retrieval Reagent (99%) for 5 min, and finally treated with RNAscope Protease III. Next, sections were hybridized with all three probes for 2 h at 40°C . To visualize the probes, sections were incubated with each of the three RNAscope Multiplex FL v2 AMP for 30 min at 40°C , and then with RNAscope Multiplex FL v2 HRP for 15 min at 40°C , and the respective TSA Vivid Dye for 30 min at 40°C , and finally the RNAscope Multiplex FL v2 HRP blocker for 15 min at 40°C . Lastly, tissue slides were mounted with Prolong Gold Antifade Mounting containing DPAI and stored in 4°C before imaging. Images were taken using a Zeiss LSM 880 Confocal Laser Scanning Microscope under the Airyscan mode (ZEN v.2.3). The *MLN*, *AGT*, and *CUBN* channels were stained with TSA Vivid Fluorophore 570, 650, and 520, and imaged using the Cy3, Cy5, and FITC filters, respectively.

Hormone concentration measurements (related to Fig. 6)

Urine and blood was collected from mouse lemurs under summer-like long days (14:10 h light:dark) and winter-like short days (10:14 h). Blood was collected in EDTA-coated capillary tubes and centrifuged at $1000\times g$ for 10 min for plasma extraction. Urine and plasma samples were stored at -80°C before follow-up assays.

Cortisol concentrations (ng/ml) were measured in duplicates from urine samples by Cortisol Urine ELISA (LDN®, catalog no. MS E-5100; standard range: 0/1 to 200 ng/ml; sensitivity: 0.47 ng/ml) following standard protocol. In brief, 10 μl urine samples, standards (0, 1, 5, 30, and 200 ng/mL), and controls were each incubated with 300 μl conjugate at 37°C for 1 h in antibody-coated microplate. Wells were then washed with wash solution and incubated with 100 μl substrate solution at room temperature for 15 min in the dark. Afterwards, 100 μl stop solution was added to each well and absorbance was read at 450 nm. Sample cortisol concentrations were calculated using the

standard curve. Urine creatinine concentration was used as an indicator of renal filtration activity to normalize urine cortisol levels. Cortisol measurements are thus expressed in ng/mg creatinine. Urine creatinine (mg/ml) was measured using Microvue™ Creatinine Elisa kit (Quidel R Corporation, catalog no. 8009) following standard protocol. In brief, urine samples, standards (0, 5, 20, 40 mmol/L), and controls were first diluted 1:40 with deionized water, and then 50 µl of each were incubated with 150 µl of Working Color Solution at room temperature for 30 min. Next, absorbance was read at 490 nm for each well and sample creatinine concentrations were calculated using the standard curve.

Thyroxine (T4, nmol/L) was assayed in plasma samples using T4 ELISA kit (LDN®, catalog no. TF E-2400; standard range: 0/25–250 nmol/L; sensitivity: 8.0 nmol/L) following standard protocol. In brief, 10 µl plasma samples, standards (adapted to 0, 10, 20, 40, 70, and 100 nmol/L), and controls were each incubated with 100 µl enzyme conjugate at room temperature for 80 min in antibody-coated microplate. Wells were then washed with wash solution and incubated with 100 µl substrate solution at room temperature for 10 min in the dark. Lastly, 100 µl stop solution was added to each well and absorbance was read at 450 nm. Sample T4 concentrations were calculated using the standard curve.

Mapping and counting transcript reads

The single-cell gene expression matrix of the mouse lemur cell atlas was obtained from the accompanying manuscript¹⁵ where methods and parameters to extract the transcript counts can be found. In this study, we used only the 10x droplet-based sequencing derived data for all analysis. In brief, the *Microcebus murinus* genome assembly (Mmur 3.0, NCBI) was used to create a genome FASTA file. Sequencing reads were processed with Cell Ranger (version 2.2, 10x Genomics) to generate cell barcodes and the gene expression matrix. We additionally counted reads for three genes (*MC1R*, *SCT*, *LHB*) that are unannotated in Mmur 3.0, NCBI. For *MC1R* and *SCT*, we used their annotation in the Ensembl *Microcebus murinus* genome. For *LHB*, we used the uTAR-scrNAseq pipeline described by Wang et al.²³ to first predict its chromosome location in the mouse lemur genome. In brief, the pipeline employs the approach of groHMM¹²³ to detect transcriptionally active regions (TARs) from aligned sequencing data and annotates these TARs as unannotated (uTARs) or annotated (aTARs) based on their overlap with the existing annotation. For the *LHB* uTAR counts, we uncovered uTARs from the mouse lemur pituitary and hypothalamus dataset and used BLASTn^{124,125} to find nucleotide sequence homology of all uTARs against human *LHB*. We found one uTAR at position NC_033681.1:19143249-19145949 with high sequence homology to human and macaque *LHB*. The *LHB* uTAR is highly differentially expressed in the expected cell type (gonadotroph). The *LHB* uTAR is located next to gene *RUVBL2*, in conservation with the co-location pattern of the genes in humans and mice²⁴. We therefore conclude that the identified *LHB* uTAR is the likely coding region of the mouse lemur *LHB* gene. We then used Drop-seq tools¹²⁶ to extract transcript counts for the three genes (*MC1R*, *SCT*, *LHB* uTAR).

Orthology and protein sequence analysis

Gene orthology mapping across human, mouse lemur, and mouse was based on the combination of both the NCBI and Ensembl ortholog databases. Details to combine the two databases were described in the accompanying manuscript¹⁵. To compare sequence similarity between orthologs of human and mouse or lemur, protein sequences were retrieved from NCBI according to protein RefSeq using the Matlab built-in function `getgenpept`. Conversion between gene ID and protein Refseq identifier was performed using “bioDBnet [<https://biodbnet.abcc.ncifcrf.gov/db/db2db.php>]”. We aligned ortholog protein sequences and used the maximal scores in the cases of multiple transcript sequences and non-one-to-one ortholog mapping. Global alignment was carried out using the Needleman–Wunsch algorithm and default parameters of the function `nwalign`.

Identification of hormone-producing and target cells

The functional concentration is different for different proteins, so we applied adaptive thresholding to determine if a gene is positively expressed in a cell type, where cell type is defined as a unique combination of the cells’ annotation and tissue of origin, as described in the accompanying Tabula *Microcebus* manuscript¹⁵. For example, vein cells of the lung and brain were considered two different cell types. Cell types that were of low quality (low gene count or transcript count) or annotated as technical doublets were removed from the analysis. For each gene, two cell-type parameters were used, mean expression level and percentage of nonzero (positive) cells. Single-cell expression levels were first normalized by total transcript counts, multiplied by 10,000, averaged across all cells in the cell type, then natural log-transformed (i.e., $\log(1 + \text{Average_UMI_count_Per_10K_Transcripts})$; note that 1 is added to the average so that genes with zero transcripts will yield zero rather than negative infinity). To determine positive expression at the cell-type level, we applied adaptive thresholding that compares the expression to the maximally expressing cell types. The algorithm involves four parameters which were selected to capture a list of well-studied cell types and hormonal genes. We first applied a low-level absolute threshold on average expression level (0.037) and percent of nonzero cells (5%) below either of which we considered the expression to be negative. Second, we calculated a robust maximal expression level of the gene by searching the high-expression levels across the atlas. Specifically, we considered the 99th percentile of the cells that passed the first thresholding to be the maximum to increase the robustness of the analysis. Lastly, we applied relative thresholding of the robust maximal level (for circulating proteins such as ligand genes at 20% and other gene types at 5%). Cell types that passed all thresholding criteria were considered to have functional expression of the gene. We used a higher relative threshold for the ligand genes because (1) ligands are secreted into the circulation so a highly expressing source overshadows a low expressing source, whereas non-ligand products of other genes (e.g., receptors, synthases, processing enzymes) function inside individual cells; (2) we noted that ligand genes were usually expressed at higher levels and were more easily affected by cross-contamination (signal spreading) inside a tissue. For hormone ligands and receptors that included multiple genes, we applied AND or OR logic gates as indicated in Supplementary Dataset 1 to determine if a cell type expressed the ligand or receptor. For an AND logic gate, a functional cell type should express all its components above the functional level; while for an OR logic gate, expression of any of its components would suffice.

Cell-type distances, clustering, and visualization

We performed hierarchical clustering of the cell types included in the mouse lemur atlas based on the transcriptional profiles of hormone ligand, synthase, modulator, and receptor genes. Analysis was carried out at the cell-type level and relative average gene expression levels were used to calculate cell-type pairwise distances. To test consistency of hormone-related gene expression among mouse lemur individuals, we separated cells from different lemurs. Because circulating immune cells sampled from different tissues were already kept as different cell types, immune cell types were not separated for different lemurs to avoid overcrowding of the data. We found that this simplification only slightly influenced the clustering results of individual cell types and did not affect the overall clustering pattern (Supplementary Fig. S5). Next, cell types were filtered to remove potentially low-quality cell types that were: (1) low in cell number, (2) technical doublets, or (3) low in transcript and/or gene count. We also manually corrected for notable cross-contamination in certain cell types. For example, almost all non-endocrine cell types of the pancreas showed high expression of insulin (*INS*) and proglucagon (*GCG*), probably caused by cross-contamination due to autolysis in the pancreas during tissue processing. We therefore removed *INS* and *GCG* expression from all non-endocrine pancreatic

cell types. In addition, we corrected contamination of *GUCA2A*, *GUCA2B*, *GIP*, *NTS*, and *SST* from stromal, endothelial, and immune cells of the intestine (small intestine and colon). Matlab built-in functions were used in the hierarchical clustering analysis. We used cosine distances to calculate cell-type pairwise distances and then applied average linkage to construct the dendrogram (cophenetic correlation coefficient = 0.81). Cell-type clusters were then divided at a threshold of 0.49 with minor manual inputs to further divide certain large clusters or merge an apparently close neighboring leaf. We obtained 74 total clusters and numbered them according to their sequence in the dendrogram shown in Fig. 2a. We also named the clusters according to the shared characteristics of its cell types. Cell types included in each cluster are listed in Supplementary Dataset 4 with the list of hormones, hormone receptors, and hormone-related genes that were expressed in the majority ($\geq 50\%$) of the cell types for each cluster.

In addition to visualizing the cell-type clustering via dendrogram, we also applied uniform manifold approximation and projection (UMAP)¹²⁷ to embed the high-dimensional expression data to 2D using a Matlab UMAP package¹²⁸. Cell-type pairwise cosine distances were used as input when generating the UMAPs.

For comparative analysis, we additionally calculated cell-type pairwise distances by the transcriptomes of all genes, the non-hormonal transcriptome, 100 random sets of PCGs (same number of genes as the hormonal genes), 100 random sets of PCGs controlling for expression variability (dispersion). These transcriptional distances were calculated similarly as the hormone-based distances were, with relative expression levels of genes used to calculate pairwise cosine distances. To select for gene sets with a similar distribution of expression specificity, we first binned genes based on their cell-type expression dispersion (i.e., variance-to-mean ratio) to 21 uniform bins and then randomly selected the same number of genes in each bin as the hormonal genes.

These transcriptional distances were compared to a benchmark cell annotation-based distance by Pearson correlation. Cell annotations, as defined in the accompanying manuscript¹⁵, was based on expression of canonical cell markers and iterative clustering with highly variable genes. This annotation-based distance was defined as an integer between 0 and 3 based on the following criteria: distance is 0 when cell types were annotated with identical names but from different tissues, 1 when our cell annotation names were different but classical histological assignments (Cell Ontology⁴⁸) were identical (i.e., different molecular subtypes), 2 when classical Cell Ontologies were different but cell types were from the same compartment (e.g., both were epithelial), and 3 if cells were different cell types and from different compartments (e.g., endothelial vs. stromal).

We additionally calculated a Cell Ontology-based distance. Each cell type was assigned a Cell Ontology term (i.e., its classical histological cell-type category) during cell-type annotation¹⁵. Cell Ontology distances were calculated as the mean of Cell Ontology embedding-based distances and text-based distances⁴⁹. Cell Ontology embedding-based distances represent distances between cell types in the Cell Ontology graph. Text-based distances were calculated using an adapted version of Sentence-BERT^{49,129}.

To estimate the quality of the clustering results, we calculated silhouette values and compared cluster average silhouette values based on only the hormone ligand genes, hormone receptor genes, or the full transcriptome. Silhouette values for a cell type i is from the equation $s(i) = \frac{b(i) - a(i)}{\max\{b(i), a(i)\}}$, for cell types belonging to a cluster with more than one member. $a(i)$ is the mean in-cluster distance, namely the mean distance between cell type i and all other cell types in the same cluster. $b(i)$ is the minimal out-cluster distance, namely the minimal mean distance between cell type i and members of other clusters.

Trajectory analysis

Analysis was performed independently for kidney samples from three mouse lemur individuals and for the cross-species spermatogenesis

dataset using an in-house program written in Matlab. To detect the vasa recta arteriole-to-venule trajectory, data were first pre-processed following the standard procedure as in Seurat¹³⁰. In brief, single-cell transcript counts for all sequenced genes were normalized to total transcript counts, log-transformed, and linearly scaled so that each gene has a mean expression of 0 and standard deviation of 1. Then, genes with high dispersion (variance-to-mean ratio) compared to other genes with the same mean expression were selected as highly variable genes for principal component analysis (PCA). Following PCA, the top 20 principal components that were not driven by extreme outlier data points or immediate early genes were used to generate a 2D UMAP using cell-cell Euclidean distances as input¹²⁷. For the cross-species spermatogenesis, we used species-integrated UMAP of the testis germ cells¹⁵. To quantify the trajectories, we detected the probability density ridge of the data points in the UMAP using automated image processing. The direction of the trajectory was manually assigned according to marker gene expression. Individual cells were aligned to the trajectory by finding the shortest connecting point to the trajectory. Data points that were too distant from the trajectory were deemed outliers and removed from the following analysis. To detect the vasa recta hormone-related genes that follow a trajectory-dependent expression pattern, we calculated the Spearman correlation coefficient between the gene expression level and 20 unimodal patterns. These pre-assigned patterns have their data smoothly changing along the trajectory and have a single peak. We let the 20 patterns have their peaks uniformly distributed from 0 to 1. This analysis tested, for each gene, whether its distribution along the trajectory follows one or more of the 20 unimodal patterns. All p values were then multi-testing corrected to detect significant genes and their associated patterns. Lastly, we compared results from the three kidney samples and kept the genes that showed consistent patterns in all three samples.

Identification of differentially expressed genes

We used the Wilcoxon rank-sum test to detect differentially expressed hormone genes among cell populations. Genes that were expressed above functional level in any of the analyzed cell populations were included in the analysis. For hormone-related genes differentially expressed during spermatogenesis, we tested whether each gene is differentially expressed in one of the three sperm cell clusters compared to the other two clusters. For the analysis of endothelial cells, we tested whether each gene is differentially expressed in the lung or brain endothelial cells compared to all other endothelial cells. For the kidney nephron analysis, we tested whether each gene is differentially expressed in one of the nephron clusters compared to the rest of the nephron epithelial cells. For the hepatocyte analysis, we tested whether each gene is differentially expressed in one subtype compared to the other in both the mouse lemur and the mouse. The mouse hepatocyte data was obtained from the Tabula Muris Senis¹¹⁴ smartseq2 plate-based sequencing of mouse hepatocytes. For the tumor cell analysis, we tested whether each gene is differentially expressed in the metastatic cells versus the MUC16+ non-ciliated uterus epithelial cells. All P values were multi-testing corrected, and then all genes with corrected P values less than 0.05 were examined to confirm consistent expression of the gene in all relevant cell types and mouse lemur individuals.

Constructing and analyzing the hormonal cell communication network

Cells with the same cell-type annotation and tissue of origin were grouped as a cell type/node. Data from different lemur individuals were merged in the analysis. Cell types that were likely low quality were removed. Edge connections were determined independently for all possible cell-type pairs. For example, if cell type A expressed a hormone ligand and cell type B expressed the corresponding hormone receptor(s), a directed edge from A to B was drawn. Note that this

allows self-loops on any cell type that expresses both the ligand and corresponding receptor. When multiple directed edges connected two cell types, they were merged for the purpose of edge counting.

Network density is defined as the number of edges divided by the number of possible edges in the network. Because the hormone and cytokine networks are directed, its network density is calculated as $\frac{N_{\text{edges}}}{N_{\text{nodes}}^2}$. For comparison, the density of an undirected network is calculated as $\frac{2 \cdot N_{\text{edges}}}{N_{\text{nodes}} \cdot (N_{\text{nodes}} + 1)}$ if it allows self-loops (e.g., protein interaction network), or $\frac{2 \cdot N_{\text{edges}}}{N_{\text{nodes}} \cdot (N_{\text{nodes}} - 1)}$ if it does not allow self-loops (e.g., genetic interaction network).

Outdegree and indegree are node features and defined as the relative number of outgoing edges (node expressing a ligand) and incoming edges (node expressing a receptor). Edge counts were normalized by cell-type abundance so that node degrees range from 0 to 100% and represent the fraction of the cell types that the node connects with by outgoing or incoming edges. To normalize the node degrees, we used a weighted cell-type abundance determined by the clustering so that each cluster contributes the same weight. This is because certain cell types like circulating immune cells are likely over-represented in the network as they appear in multiple tissues and would be categorized as different cell types by our definition. We did not merge circulating cell types from different tissues because it is challenging for some cell types like T cells to determine whether they are circulating or potentially tissue-specific or tissue-resident. We also tried simply normalizing the node degree by the total number of nodes; similar conclusions were reached using either method.

Calculating generality scores for hormone ligands and receptors

To calculate generality scores for the hormone ligands and receptors, we counted the cell types that express the ligand or receptor. Cell types that were likely low quality were removed from the analysis. Cell-type counts were normalized by cell-type abundances similarly as was the node degree, so that the generality score was not dominated by over-represented cell types. In comparison, we also counted the cell-type clusters that express the hormone ligands and receptors. Here, we defined that a gene was expressed in a cell-type cluster if more than 50% of the cell types in the cluster positively expressed the gene.

To analyze the distribution of generality scores, we tested if the distribution followed normal, exponential, lognormal, or gamma distributions. We first performed parametric distribution fitting and then performed Kolmogorov–Smirnov tests comparing the fitted versus data cumulative distribution functions. This analysis used Matlab built-in functions `fitdist` and `kstest`. In addition, we tested if the data followed a power-law distribution using `plfit` and `plpva` functions¹³¹.

Calculating target cell Jaccard indices for different receptors that bind to the same ligand

We calculated Jaccard indices for pairs of receptors that (1) can bind to the same ligand as described in Supplementary Dataset 1, and (2) were both expressed in at least one atlas cell type. Jaccard index here is calculated as the number of cell types that express both receptors divided by the number of cell types that express either of the receptors.

Network perturbation analysis

We performed two types of network perturbations: degree-preserving random rewiring and random edge removal. For degree-preserving random rewiring, we applied the algorithm developed by Maslov and Sneppen⁸². The algorithm starts with the original network and performs repeated rewiring steps. For each rewiring, it randomly identifies two edges (e.g., $A \rightarrow B$ and $C \rightarrow D$) and swaps the connections (i.e., $A \rightarrow D$ and $C \rightarrow B$). This allows constructing a random network while preserving the node indegree and outdegree of the original network. For the

perturbation by edge removal, we randomly selected 10% of the edge types (ligand-receptor pairs) and removed these edges from the original network. Note for this analysis, multiple directed edges connecting the same cell-type pairs were not merged. Therefore, the connection between two cell types would be removed only if all of its redundant edges (of different ligand-receptor pairs) were selected to be removed.

Cross-species comparisons of hormonal gene expression

We compared cells of the lung, skeletal muscle, liver, testis, bone marrow, and spleen. All lemur data was from the 10x data of the accompanying *Tabula Microcebus* manuscript¹⁵. Human data were from the 10x data of the *Tabula Sapiens*¹²⁰, except for the lung which we used the 10x data from the Human Lung Cell Atlas¹³² and the testis which we used drop-seq data from ref. 133. Mouse data were from 10x data of the *Tabula Muris Senis*¹⁴ except for the testis which we used 10x data from ref. 134. For lung and muscle, all cell types were included in the analysis, whereas we only analyzed the epithelial cells for the liver, immune cells for the bone marrow and spleen, and germ cells for the testis. If a dataset contained cells from early or postnatal development, these cells were excluded and only cells from adult animals were used, for consistency. The number of individuals analyzed are as follows: three donors for human spleen, bone marrow, lung; four for human testes; two for human liver, abdominal muscle; three for lemur spleen, bone marrow, and liver; four for lemur lung; one for lemur limb muscle and testes; ten for mouse spleen; thirteen for mouse bone marrow; twelve for mouse limb muscle; seven for mouse liver; ten for mouse lung; and two for mouse testes. We used one-to-one orthologs across all three species. This resulted in ~15,000 genes (324 hormonal genes), ~13,000 of which were included in all scRNAseq datasets (295 hormonal genes).

To unify cell-type annotations, human and mouse datasets were first separately re-annotated according to the same pipeline and marker genes as for the lemur data. Cells that were deemed low quality (i.e., low in transcript and/or gene count) and technical doublets were removed from downstream analysis. Next, to ensure cell types are comparable across species, we applied Portal¹³⁵ to integrate data (one-to-one orthologs only) from different species. Portal projects data into a space that minimizes species differences, from which an integrated UMAP is generated to visualize cell clustering from different species. Integration was performed separately for each tissue, except for bone marrow and spleen which were integrated jointly. We manually inspected each integration UMAP and ensured that cells of the same type showed reasonable cross-species co-clustering and separation from other cell types. We also made small modifications to the cell annotations/clustering during this process to unify annotations across species. For example, proliferating cells might co-cluster with the main non-proliferating population in the original dataset if the number of cells are too few, but cluster separately with the proliferating populations of the other species in the integrated UMAP. In such a scenario, we would separately annotate these cells as a proliferating subtype. Additional details to compile the cross-species scRNAseq datasets were described in the accompanying manuscript¹⁵.

Cell types with more than 15 cells in all three species were then used for the cross-species comparisons, resulting in a total of 62 orthologous cell types ($62 \times 3 = 186$ cell-type entries in all three species). Cell-type average expressions were calculated separately for each species. Note that cellular expression levels in the species-integrated dataset were normalized by the sum of only the one-to-one orthologs, rather than all the genes, thus at high levels compared to the non-integrated data. Cross-species similarity was calculated separately for individual genes. We first identified genes that are at least moderately expressed in the analyzed cell types (≥ 3 cell-type entries with mean expression > 1), which resulted in a total of 90 genes for follow-up analysis. Expression levels were then normalized by the maximally

expressed cell type in each species and cross-species correlation coefficients between human and lemur ($r(\text{human, lemur})$) and between human and mouse ($r(\text{human, mouse})$) were calculated. $\Delta r = r(\text{human, lemur}) - r(\text{human, mouse})$ was calculated. Lastly, we identified genes that are more conserved between humans and lemurs compared to mice ($\Delta r > 0.5$), and in contrast genes that are more conserved between humans and mice compared to lemurs ($\Delta r < -0.5$). To compare overall similarity of transcriptional profiles of the hormonal genes or all genes, we concatenated cell-type expression profiles for individual genes and calculated correlation coefficients between human and lemur and between human and mouse. P values of the difference in correlation coefficients were calculated using Fisher's Z-transformation¹³⁶. Integrated cross-species data are available at Stanford Digital Repository (see "Data and Code Availability"), providing detailed information of individual cell barcodes, original datasets, individuals, cell annotation assigned in original publications, revised/unified annotation used for cross-species comparison, coordinates for the Portal-integrated UMAPs, as well as per cell read count for all one-to-one orthologs.

Statistics and reproducibility

A total of four mouse lemurs (L1-4) were used in this study. The sample size was determined by the availability of the animals in accordance with the approved animal protocol, and no statistical method was used to predetermine sample size. For the RNAscope experiments, kidney samples from L4 were used based on availability. Two tissue sections were stained with similar results.

In the analysis of the scRNAseq data, we excluded cell types that were (1) low in cell number, (2) technical doublets, or (3) low in transcript and/or gene count. In addition, we excluded several notable cross-contamination genes when clustering the cell types by hormonal genes. In the cross-species analysis, cells that were deemed low quality (i.e., low in transcript and/or gene count) or technical doublets were removed from the integration analysis. In addition, if a dataset included cells sampled from animals during early or postnatal development (from mouse datasets), these cells were not used, and we only analyzed cells sampled from adult animals for consistency. Cell types (after unification across species) with fewer than 15 cells in any of the species were excluded from the downstream analysis of evolutionary comparisons. Additional details on data exclusions are described in "Methods".

Reporting summary

Further information on research design is available in the Nature Portfolio Reporting Summary linked to this article.

Data availability

Tabula Microcebus mouse lemur scRNAseq gene expression counts/UMI tables, and cellular metadata used in this study are available on "figshare [https://figshare.com/projects/Tabula_Microcebus/112227]", and can be explored interactively using cellxgene and in dot plot format on the "Tabula Microcebus web portal [<https://tabula-microcebus.ds.czbiohub.org/>]", For the cross-species comparison, human data were from the 10x data of the "Tabula Sapiens for the liver, spleen, and bone marrow [https://figshare.com/projects/Tabula_Sapiens/100973]", 10x data of the "Human Lung Cell Atlas for the lung [<https://www.synapse.org/#1Synapse:syn21041850/wiki/600865>]", and the drop-seq data from "Shami et al. for the testis [<https://www.ncbi.nlm.nih.gov/geo/query/acc.cgi?acc=GSE142585>]", Mouse data were from 10x data of the "Tabula Muris Senis [https://figshare.com/articles/dataset/Processed_files_to_use_with_scanpy/8273102/2]" except for the testis which we used 10x data from "Ernst et al. [<https://www.ebi.ac.uk/biostudies/arrayexpress/studies/E-MTAB-6946>]", Metadata generated in this study, including the integrated cross-species metadata, have been deposited in the "Stanford Digital Repository [<https://purl.stanford.edu/yp860tc1411>]", <https://doi.org/10.25740/yp860tc1411>. Selected data discussed in the manuscript, including the assembled hormonal gene table and the list of analyzed cell types and their clustering results, are also provided as Supplementary Datasets. All other data supporting the findings of this study are available within the article and its supplementary files. Any additional requests for information can be directed to, and will be fulfilled by, the corresponding authors. Source data are provided with this paper.

Computer codes have been deposited in the "Stanford Digital Repository [<https://purl.stanford.edu/yp860tc1411>]", <https://doi.org/10.25740/yp860tc1411>.

Code availability

Computer codes have been deposited in the "Stanford Digital Repository [<https://purl.stanford.edu/yp860tc1411>]", <https://doi.org/10.25740/yp860tc1411>.

References

1. Bayliss, W. M. & Starling, E. H. The mechanism of pancreatic secretion. *J. Physiol.* **28**, 325–353 (1902).
2. Takei, Y., Ando, H. & Tsutsui, K. *Handbook of Hormones: Comparative Endocrinology for Basic and Clinical Research* (Academic Press, 2015).
3. Tata, J. R. One hundred years of hormones. *EMBO Rep.* **6**, 490–496 (2005).
4. Lewis, G. F. & Brubaker, P. L. The discovery of insulin revisited: lessons for the modern era. *J. Clin. Investig.* **131**, e142239 (2021).
5. Horby, P. et al. Dexamethasone in hospitalized patients with Covid-19. *New Engl. J. Med.* **384**, 693–704 (2021).
6. Sterne, J. A. C. et al. Association Between administration of systemic corticosteroids and mortality among critically ill patients with COVID-19: a meta-analysis. *J. Am. Med. Assoc.* **324**, 1330–1341 (2020).
7. Scheja, L. & Heeren, J. The endocrine function of adipose tissues in health and cardiometabolic disease. *Nat. Rev. Endocrinol.* **15**, 507–524 (2019).
8. Jabbour, H. N., Kelly, R. W., Fraser, H. M. & Critchley, H. O. D. Endocrine regulation of menstruation. *Endocr. Rev.* **27**, 17–46 (2006).
9. Deb, A., Deshmukh, B., Ramteke, P., Bhati, F. K. & Bhat, M. K. Resistin: a journey from metabolism to cancer. *Transl. Oncol.* **14**, 101178 (2021).
10. Ezran, C. et al. The mouse lemur, a genetic model organism for primate biology, behavior, and health. *Genetics* **206**, 651–664 (2017).
11. Bons, N., Rieger, F., Prudhomme, D., Fisher, A. & Krause, K. H. *Microcebus murinus*: a useful primate model for human cerebral aging and Alzheimer's disease? *Genes Brain Behav.* **5**, 120–130 (2006).
12. Languille, S. et al. The grey mouse lemur: a non-human primate model for ageing studies. *Ageing Res. Rev.* **11**, 150–162 (2012).
13. Kraska, A. et al. Age-associated cerebral atrophy in mouse lemur primates. *Neurobiol. Aging* **32**, 894–906 (2011).
14. Pifferi, F. et al. Promoting healthspan and lifespan with caloric restriction in primates. *Commun. Biol.* **2**, 107 (2019).
15. The Tabula Microcebus Consortium. Tabula Microcebus: a transcriptomic cell atlas of mouse lemur, an emerging primate model organism. Preprint at *bioRxiv* <https://doi.org/10.1101/2021.12.12.469460> (2021).
16. The Tabula Microcebus Consortium et al. Mouse lemur transcriptomic atlas elucidates primate genes, physiology, disease, and evolution. Preprint at *bioRxiv* <https://doi.org/10.1101/2022.08.06.503035> (2022).
17. Casey, K. M., Karanewsky, C. J., Pendleton, J. L., Krasnow, M. R. & Albertelli, M. A. Fibrous osteodystrophy, chronic renal disease, and uterine adenocarcinoma in aged gray mouse Lemurs (*Microcebus murinus*). *Comp. Med.* **71**, 256–266 (2021).

18. Kastin, A. *Handbook of Biologically Active Peptides* (Academic Press, 2013).
19. Romere, C. et al. Asprosin, a fasting-induced glucogenic protein hormone. *Cell* **165**, 566–579 (2016).
20. Itoh, N., Ohta, H. & Konishi, M. Endocrine FGFs: evolution, physiology, pathophysiology, and pharmacotherapy. *Front. Endocrinol.* **6**, 154 (2015).
21. Hammond, G. L. Plasma steroid-binding proteins: primary gatekeepers of steroid hormone action. *J. Endocrinol.* **230**, R13–R25 (2016).
22. Hammond, G. L., Hill, L. A. & Round, P. W. Roles of plasma binding proteins in modulation of hormone action and metabolism. In *Encyclopedia of Endocrine Diseases*, Second edition. (ed. Ilpo Huhtaniemi, L. M.) 51–60 (Academic Press, 2019).
23. Wang, M. F. Z. et al. Uncovering transcriptional dark matter via gene annotation independent single-cell RNA sequencing analysis. *Nat. Commun.* **12**, 1–10 (2021).
24. Parfait, B. et al. Human TIP49b/RUVBL2 gene: genomic structure, expression pattern, physical link to the human CGB/LHB gene cluster on chromosome 19q13.3. *Ann. Genet.* **43**, 69–74 (2000).
25. Riddle, O., Bates, R. W. & Dykshorn, S. W. The preparation, identification and assay of prolactin—a hormone of the anterior pituitary. *Am. J. Physiol.-Leg. Content* **105**, 191–216 (1933).
26. Bole-Feysot, C., Goffin, V., Edery, M., Binart, N. & Kelly, P. A. Prolactin (PRL) and its receptor: actions, signal transduction pathways and phenotypes observed in PRL receptor knockout mice. *Endocr. Rev.* **19**, 225–268 (1998).
27. Tovar, S. & Diéguez, C. Prolactin and energy homeostasis: pathophysiological mechanisms and therapeutic considerations. *Endocrinology* **155**, 659–662 (2014).
28. Paré, P. et al. Molecular evolutionary insights from PRLR in mammals. *Gen. Comp. Endocrinol.* **309**, 113791 (2021).
29. Giroud, S. et al. The grey mouse lemur uses season-dependent fat or protein sparing strategies to face chronic food restriction. *PLoS ONE* **5**, e8823 (2010).
30. Terrien, J. et al. Metabolic and genomic adaptations to winter fattening in a primate species, the grey mouse lemur (*Microcebus murinus*). *Int. J. Obes.* **42**, 221–230 (2018).
31. Perret, M. & Aujard, F. Regulation by photoperiod of seasonal changes in body mass and reproductive function in gray mouse lemurs (*Microcebus murinus*): differential responses by sex. *Int. J. Primatol.* **22**, 5–24 (2001).
32. Maeda, K. et al. cDNA cloning and expression of a novel adipose specific collagen-like factor, apM1 (AdiPose Most abundant Gene transcript 1). *Biochem. Biophys. Res. Commun.* **221**, 286–289 (1996).
33. Zhang, Y. et al. Positional cloning of the mouse obese gene and its human homologue. *Nature* **372**, 425–432 (1994).
34. Galic, S., Oakhill, J. S. & Steinberg, G. R. Adipose tissue as an endocrine organ. *Mol. Cell. Endocrinol.* **316**, 129–139 (2010).
35. Ruan, H. & Dong, L. Q. Adiponectin signaling and function in insulin target tissues. *J. Mol. Cell Biol.* **8**, 101–109 (2016).
36. Yamauchi, T. et al. Cloning of adiponectin receptors that mediate anti-diabetic metabolic effects. *Nature* **423**, 762–769 (2003).
37. He, J., Irwin, D. M., Chen, R. & Zhang, Y.-P. Stepwise loss of motilin and its specific receptor genes in rodents. *J. Mol. Endocrinol.* **44**, 37–44 (2010).
38. Sanger, G. J., Wang, Y., Hobson, A. & Broad, J. Motilin: towards a new understanding of the gastrointestinal neuropharmacology and therapeutic use of motilin receptor agonists. *Br. J. Pharmacol.* **170**, 1323–1332 (2013).
39. Hu, Q., Tan, H. & Irwin, D. M. Evolution of the vertebrate resistin gene family. *PLoS One* **10**, e0130188 (2015).
40. Schwartz, D. R. & Lazar, M. A. Human resistin: found in translation from mouse to man. *Trends Endocrinol. Metab.* **22**, 259–265 (2011).
41. Zhang, X. et al. Neuropeptidomic analysis establishes a major role for prohormone convertase-2 in neuropeptide biosynthesis. *J. Neurochem.* **112**, 1168–1179 (2010).
42. Seidah, N. G. The proprotein convertases, 20 years later. *Methods Mol. Biol.* **768**, 23–57 (2011).
43. Sandoval, D. A. & D'Alessio, D. A. Physiology of proglucagon peptides: role of glucagon and GLP-1 in health and disease. *Physiol. Rev.* **95**, 513–548 (2015).
44. Wardlaw, S. L. Hypothalamic proopiomelanocortin processing and the regulation of energy balance. *Eur. J. Pharmacol.* **660**, 213–219 (2011).
45. Allard, J. B. & Duan, C. IGF-binding proteins: why do they exist and why are there so many? *Front. Endocrinol.* **9**, 117 (2018).
46. Bouillon, R., Schuit, F., Antonio, L. & Rastinejad, F. Vitamin D binding protein: a historic overview. *Front. Endocrinol.* **10**, 910 (2020).
47. Schneider, C., O'Leary, C. E. & Locksley, R. M. Regulation of immune responses by tuft cells. *Nat. Rev. Immunol.* **19**, 584–593 (2019).
48. Smith, B. et al. The OBO Foundry: coordinated evolution of ontologies to support biomedical data integration. *Nat. Biotechnol.* **25**, 1251–1255 (2007).
49. Wang, S. et al. Leveraging the cell ontology to classify unseen cell types. *Nat. Commun.* **12**, 5556 (2021).
50. Griswold, M. D. Spermatogenesis: the commitment to meiosis. *Physiol. Rev.* **96**, 1–17 (2016).
51. Smith, L. B. & Walker, W. H. The regulation of spermatogenesis by androgens. *Semin. Cell Dev. Biol.* **30**, 2–13 (2014).
52. Ruwanpura, S. M., McLachlan, R. I. & Meachem, S. J. Hormonal regulation of male germ cell development. *J. Endocrinol.* **205**, 117–131 (2010).
53. Lishko, P. V., Botchkina, I. L. & Kirichok, Y. Progesterone activates the principal Ca²⁺ channel of human sperm. *Nature* **471**, 387–391 (2011).
54. Lue, Y. et al. Functional role of progestin and the progesterone receptor in the suppression of spermatogenesis in rodents. *Andrology* **1**, 308–317 (2013).
55. Burnicka-Turek, O. et al. Inactivation of insulin-like factor 6 disrupts the progression of spermatogenesis at late meiotic prophase. *Endocrinology* **150**, 4348–4357 (2009).
56. Giesecke, T. et al. Vasopressin increases urinary acidification via V1a receptors in collecting duct intercalated cells. *J. Am. Soc. Nephrol.* **30**, 946–961 (2019).
57. Pannabecker, T. L. & Dantzier, W. H. Three-dimensional architecture of inner medullary vasa recta. *Am. J. Physiol. Ren. Physiol.* **290**, F1355–F1366 (2006).
58. Kenig-Kozlovsky, Y. et al. Ascending vasa recta are angiopoietin/tie2-dependent lymphatic-like vessels. *J. Am. Soc. Nephrol.* **29**, 1097–1107 (2018).
59. Barry, D. M. et al. Molecular determinants of nephron vascular specialization in the kidney. *Nat. Commun.* **10**, 5705 (2019).
60. Backes, F. J. et al. Estrogen receptor-alpha as a predictive biomarker in endometrioid endometrial cancer. *Gynecol. Oncol.* **141**, 312–317 (2016).
61. Shen, F., Gao, Y., Ding, J. & Chen, Q. Is the positivity of estrogen receptor or progesterone receptor different between type 1 and type 2 endometrial cancer? *Oncotarget* **8**, 506–511 (2017).
62. Nakanishi, M. & Rosenberg, D. W. Multifaceted roles of PGE2 in inflammation and cancer. *Semin. Immunopathol.* **35**, 123–137 (2013).
63. Ke, J. et al. Prostaglandin E2 (PGE2) promotes proliferation and invasion by enhancing SUMO-1 activity via EP4 receptor in endometrial cancer. *Tumour Biol.* **37**, 12203–12211 (2016).

64. Lee, J. O. et al. Resistin, a fat-derived secretory factor, promotes metastasis of MDA-MB-231 human breast cancer cells through ERM activation. *Sci. Rep.* **6**, 18923 (2016).
65. Groneberg, D. A., Springer, J. & Fischer, A. Vasoactive intestinal polypeptide as mediator of asthma. *Pulm. Pharmacol. Ther.* **14**, 391–401 (2001).
66. Barnes, K. & Turner, A. J. The endothelin system and endothelin-converting enzyme in the brain: molecular and cellular studies. *Neurochem. Res.* **22**, 1033–1040 (1997).
67. Wilhelms, D. B. et al. Deletion of prostaglandin E2 synthesizing enzymes in brain endothelial cells attenuates inflammatory fever. *J. Neurosci.* **34**, 11684–11690 (2014).
68. Engström, L. et al. Lipopolysaccharide-induced fever depends on prostaglandin E2 production specifically in brain endothelial cells. *Endocrinology* **153**, 4849–4861 (2012).
69. Frankenstein, Z., Alon, U. & Cohen, I. R. The immune-body cytokine network defines a social architecture of cell interactions. *Biol. Direct* **1**, 32 (2006).
70. Giot, L. et al. A protein interaction map of *Drosophila melanogaster*. *Science* **302**, 1727–1736 (2003).
71. Yook, S. H., Oltvai, Z. N. & Barabási, A. L. Functional and topological characterization of protein interaction networks. *Proteomics* **4**, 928–942 (2004).
72. Rolland, T. et al. A proteome-scale map of the human interactome network. *Cell* **159**, 1212–1226 (2014).
73. Costanzo, M. et al. The genetic landscape of a cell. *Science* **327**, 425–431 (2010).
74. Barabási, A.-L. Scale-free and hierarchical structures in complex networks. *AIP Conf. Proc.* **661**, 1–16 (2003).
75. Iams, W. T. & Lovly, C. M. Molecular pathways: clinical applications and future direction of insulin-like growth factor-1 receptor pathway blockade. *Clin. Cancer Res.* **21**, 4270–4277 (2015).
76. Ghosh, P., Dahms, N. M. & Kornfeld, S. Mannose 6-phosphate receptors: new twists in the tale. *Nat. Rev. Mol. Cell Biol.* **4**, 202–212 (2003).
77. Larhammar, D. & Salaneck, E. Molecular evolution of NPY receptor subtypes. *Neuropeptides* **38**, 141–151 (2004).
78. Kilpatrick, L. E., Humphrys, L. J. & Holliday, N. D. A G protein-coupled receptor dimer imaging assay reveals selectively modified pharmacology of neuropeptide Y Y1/Y5 receptor heterodimers. *Mol. Pharmacol.* **87**, 718–732 (2015).
79. Gehlert, D. R., Schober, D. A., Morin, M. & Berglund, M. M. Co-expression of neuropeptide Y Y1 and Y5 receptors results in heterodimerization and altered functional properties. *Biochem. Pharmacol.* **74**, 1652–1664 (2007).
80. Almabouada, F. et al. Adiponectin receptors form homomers and heteromers exhibiting distinct ligand binding and intracellular signaling properties. *J. Biol. Chem.* **288**, 3112–3125 (2013).
81. Keshvari, S. et al. Characterisation of the adiponectin receptors: the non-conserved N-terminal region of AdipoR2 prevents its expression at the cell-surface. *Biochem. Biophys. Res. Commun.* **432**, 28–33 (2013).
82. Maslov, S. & Sneppen, K. Specificity and stability in topology of protein networks. *Science* **296**, 910–913 (2002).
83. Dwyer, A. A. & Quinton, R. Anatomy and physiology of the hypothalamic-pituitary-gonadal (HPG) axis. In *Advanced Practice in Endocrinology Nursing* (eds Llahana, S. et al.). Springer, Cham, 839–852 (2019).
84. Martín-Estal, I., de la Garza, R. G. & Castilla-Cortázar, I. Intrauterine growth retardation (IUGR) as a novel condition of insulin-like growth factor-1 (IGF-1) deficiency. *Rev. Physiol. Biochem. Pharmacol.* **170**, 1–35 (2016).
85. Inagaki, T. et al. Inhibition of growth hormone signaling by the fasting-induced hormone FGF21. *Cell Metab.* **8**, 77–83 (2008).
86. Hartig, S. M. & Cox, A. R. Paracrine signaling in islet function and survival. *J. Mol. Med.* **98**, 451–467 (2020).
87. Habegger, K. M. et al. The metabolic actions of glucagon revisited. *Nat. Rev. Endocrinol.* **6**, 689–697 (2010).
88. Habegger, K. M. et al. Fibroblast growth factor 21 mediates specific glucagon actions. *Diabetes* **62**, 1453–1463 (2013).
89. Mu, J. et al. FGF21 analogs of sustained action enabled by orthogonal biosynthesis demonstrate enhanced antidiabetic pharmacology in rodents. *Diabetes* **61**, 505–512 (2012).
90. Mancuso, E. et al. Insulin-like growth factor-1 is a negative modulator of glucagon secretion. *Oncotarget* **8**, 51719–51732 (2017).
91. Kopchick, J. J., Berryman, D. E., Puri, V., Lee, K. Y. & Jorgensen, J. O. L. The effects of growth hormone on adipose tissue: old observations, new mechanisms. *Nat. Rev. Endocrinol.* **16**, 135–146 (2020).
92. Carré, N. & Binart, N. Prolactin and adipose tissue. *Biochimie* **97**, 16–21 (2014).
93. Iwen, K. A. et al. Melanocortin crosstalk with adipose functions: ACTH directly induces insulin resistance, promotes a pro-inflammatory adipokine profile and stimulates UCP-1 in adipocytes. *J. Endocrinol.* **196**, 465–472 (2008).
94. Sarmiento-Cabral, A. et al. Adipokines (leptin, adiponectin, resistin) differentially regulate all hormonal cell types in primary anterior pituitary cell cultures from two primate species. *Sci. Rep.* **7**, 43537 (2017).
95. Ferrell, J. E. Jr. Self-perpetuating states in signal transduction: positive feedback, double-negative feedback and bistability. *Curr. Opin. Cell Biol.* **14**, 140–148 (2002).
96. Tezze, C., Romanello, V. & Sandri, M. FGF21 as modulator of metabolism in health and disease. *Front. Physiol.* **10**, 419 (2019).
97. Kineman, R. D., Del Rio-Moreno, M. & Sarmiento-Cabral, A. 40 Years of IGF1: understanding the tissue-specific roles of IGF1/IGF1R in regulating metabolism using the Cre/loxP. *Syst. J. Mol. Endocrinol.* **61**, T187–T198 (2018).
98. Petter-Rousseaux, A. Age of *Microcebus murinus* at the onset of testicular development: Preliminary observations on photoperiodic effect. *Ann. Biol. Anim. Biochem. Biophys.* **19**, 1801–1806 (1979).
99. Perret, M. Environmental and social determinants of sexual function in the male lesser mouse lemur (*Microcebus murinus*). *Folia Primatol.* **59**, 1–25 (1992).
100. Epelbaum, J. & Terrien, J. Mini-review: aging of the neuroendocrine system: Insights from nonhuman primate models. *Prog. Neuro-psychopharmacol. Biol. Psychiatry* **100**, 109854 (2020).
101. Murat, F. et al. The molecular evolution of spermatogenesis across mammals. *Nature* **613**, 308–316 (2023).
102. Champaneria, M. C., Modlin, I. M., Kidd, M. & Eick, G. N. Friedrich Feyrter: a precise intellect in a diffuse system. *Neuroendocrinology* **83**, 394–404 (2006).
103. Karin, O. et al. A new model for the HPA axis explains dysregulation of stress hormones on the timescale of weeks. *Mol. Syst. Biol.* **16**, e9510 (2020).
104. Perret, M. & Aujard, F. Daily hypothermia and torpor in a tropical primate: synchronization by 24-h light-dark cycle. *Am. J. Physiol.-Regul. Integr. Comp. Physiol.* **281**, R1925–R1933 (2001).
105. Gwinner, E. *Circannual Rhythms: Endogenous Annual Clocks in the Organization of Seasonal Processes* (Springer, 2011).
106. Lincoln, G. A brief history of circannual time. *J. Neuroendocrinol.* **31**, e12694 (2019).
107. Tendler, A. et al. Hormone seasonality in medical records suggests circannual endocrine circuits. *Proc. Natl. Acad. Sci. USA* **118**, e2003926118 (2021).
108. Sailani, M. R. et al. Deep longitudinal multiomics profiling reveals two biological seasonal patterns in California. *Nat. Commun.* **11**, 4933 (2020).

109. Dopico, X. C. et al. Widespread seasonal gene expression reveals annual differences in human immunity and physiology. *Nat. Commun.* **6**, 7000 (2015).
110. Moriyama, M., Hugentobler, W. J. & Iwasaki, A. Seasonality of respiratory viral infections. *Annu. Rev. Virol.* **7**, 83–101 (2020).
111. Marti-Soler, H. et al. Seasonal variation of overall and cardiovascular mortality: a study in 19 countries from different geographic locations. *PLoS ONE* **9**, e113500 (2014).
112. Kurlansik, S. L. & Ibay, A. D. Seasonal affective disorder. *Am. Fam. Physician* **86**, 1037–1041 (2012).
113. Chen, G., Ning, B. & Shi, T. Single-cell RNA-Seq technologies and related computational data analysis. *Front. Genet.* **10**, 317 (2019).
114. Tabula Muris Consortium. A single-cell transcriptomic atlas characterizes ageing tissues in the mouse. *Nature* **583**, 590–595 (2020).
115. The Tabula Muris Consortium Single-cell transcriptomics of 20 mouse organs creates a Tabula Muris. *Nature* **562**, 367–372 (2018).
116. Han, X. et al. Mapping the mouse cell atlas by Microwell-Seq. *Cell* **172**, 1091–1107.e17 (2018).
117. Cao, C. et al. Comprehensive single cell transcriptome lineages of a proto-vertebrate. *Nature* **571**, 349–354 (2019).
118. Qu, J. et al. A reference single-cell regulomic and transcriptomic map of cynomolgus monkeys. *Nat. Commun.* **13**, 4069 (2022).
119. Han, L. et al. Cell transcriptomic atlas of the non-human primate *Macaca fascicularis*. *Nature* **604**, 723–731 (2022).
120. Tabula Sapiens Consortium* et al. The Tabula Sapiens: a multiple-organ, single-cell transcriptomic atlas of humans. *Science* **376**, eabl4896 (2022).
121. van den Beld, A. W. et al. The physiology of endocrine systems with ageing. *Lancet Diabetes Endocrinol.* **6**, 647–658 (2018).
122. National Research Council. *Guide for the Care and Use of Laboratory Animals*, Eighth edition (National Research Council, 2010).
123. Chae, M., Danko, C. G. & Lee Kraus, W. groHMM: a computational tool for identifying unannotated and cell type-specific transcription units from global run-on sequencing data. *BMC Bioinforma.* **16**, 1–16 (2015).
124. Johnson, M. et al. NCBI BLAST: a better web interface. *Nucleic Acids Res.* **36**, W5–W9 (2008).
125. Altschul, S. F., Gish, W., Miller, W., Myers, E. W. & Lipman, D. J. Basic local alignment search tool. *J. Mol. Biol.* **215**, 403–410 (1990).
126. Macosko, E. Z. et al. Highly parallel genome-wide expression profiling of individual cells using nanoliter droplets. *Cell* **161**, 1202–1214 (2015).
127. McInnes, L., Healy, J. & Melville, J. UMAP: Uniform Manifold Approximation and Projection. *JOSS.* **3**, 29, 861 (2018).
128. Meehan, C., Ebrahimi, J., Moore, W. & Meehan, S. Uniform manifold approximation and projection (UMAP). *MATLAB Central File Exchange* <https://www.mathworks.com/matlabcentral/fileexchange/71902> (2021).
129. Reimers, N. & Gurevych, I. Sentence-BERT: sentence embeddings using Siamese BERT-Networks <https://doi.org/10.48550/arXiv.1908.10084> (2019).
130. Butler, A., Hoffman, P., Smibert, P., Papalexi, E. & Satija, R. Integrating single-cell transcriptomic data across different conditions, technologies, and species. *Nat. Biotechnol.* **36**, 411–420 (2018).
131. Clauset, A., Shalizi, C. R. & Newman, M. E. J. Power-law distributions in empirical data. *SIAM Rev. Soc. Ind. Appl. Math.* **51**, 661–703 (2009).
132. Travaglini, K. J. et al. A molecular cell atlas of the human lung from single-cell RNA sequencing. *Nature* **587**, 619–625 (2020).
133. Shami, A. N. et al. Single-cell RNA sequencing of human, macaque, and mouse testes uncovers conserved and divergent features of mammalian spermatogenesis. *Dev. Cell* **54**, 529–547.e12 (2020).
134. Ernst, C., Eling, N., Martinez-Jimenez, C. P., Marioni, J. C. & Odom, D. T. Staged developmental mapping and X chromosome transcriptional dynamics during mouse spermatogenesis. *Nat. Commun.* **10**, 1251 (2019).
135. Zhao, J. et al. Adversarial domain translation networks for integrating large-scale atlas-level single-cell datasets. *Nat. Comput. Sci.* **2**, 317–330 (2022).
136. Fisher, R. A. Frequency distribution of the values of the correlation coefficient in samples from an indefinitely large population. *Biometrika* **10**, 507–521 (1915).
137. Noiret, A. et al. Sex-specific response to caloric restriction after reproductive investment in *Microcebus murinus*: an integrative approach. *Front. Physiol.* **11**, 506 (2020).
138. Perret, M. & Aujard, F. Aging and season affect plasma dehydroepiandrosterone sulfate (DHEA-S) levels in a primate. *Exp. Gerontol.* **40**, 582–587 (2005).
139. Dal-Pan, A. et al. Caloric restriction or resveratrol supplementation and ageing in a non-human primate: first-year outcome of the RESTRIKAL study in *Microcebus murinus*. *Age* **33**, 15–31 (2011).
140. Petter-Rousseaux, A. & Picon, R. Annual variation in the plasma testosterone in *Microcebus murinus*. *Folia Primatol.* **36**, 183–190 (1981).
141. Schilling, A. & Perret, M. Removal of the olfactory bulbs modifies the gonadal responses to photoperiod in the lesser mouse lemur (*Microcebus murinus*). *Biol. Reprod.* **49**, 58–65 (1993).
142. Petter-Rousseaux, A. Annual variations in the plasma thyroxine level in *Microcebus murinus*. *Gen. Comp. Endocrinol.* **55**, 405–409 (1984).
143. Perret, M. & Predine, J. Effects of long-term grouping on serum cortisol levels in *Microcebus murinus* (Prosimii). *Horm. Behav.* **18**, 346–358 (1984).
144. Aujard, F., Bluet-Pajot, M. T., Zizzari, P., Perret, M. & Epelbaum, J. IGF-1: a marker of individual life-span in a primate. *Ageing Res.* **1**, e2 (2010).
145. Aujard, F. et al. Artificially accelerated aging by shortened photoperiod alters early gene expression (Fos) in the suprachiasmatic nucleus and sulfatoxymelatonin excretion in a small primate, *Microcebus murinus*. *Neuroscience* **105**, 403–412 (2001).
146. Giroud, S. et al. Gut hormones in relation to body mass and torpor pattern changes during food restriction and re-feeding in the gray mouse lemur. *J. Comp. Physiol. B* **179**, 99–111 (2009).
147. Dal-Pan, A., Blanc, S. & Aujard, F. Resveratrol suppresses body mass gain in a seasonal non-human primate model of obesity. *BMC Physiol.* **10**, 11 (2010).

Acknowledgements

We are grateful to Sandra Schmid, Uri Alon, Chaitan Khosla, Mathieu Lemaire, the Krasnow lab, and the Ferrell lab for helpful discussions and comments on the manuscript. This work is supported by NIH grant R35 GM131792 to J.E. Ferrell, funding from Wall Center to M.A. Krasnow, and a fellowship from the Wu Tsai Neurosciences Institute to S. Liu. M.A. Krasnow is an investigator of the Howard Hughes Medical Institute.

Author contributions

S. Liu, M.A. Krasnow, and J.E. Ferrell conceived the project. S. Liu designed and performed all the analyses with input from C. Ezran, Z. Li, C.S. Kuo, J. Epelbaum, J. Terrien, M.A. Krasnow, and J.E. Ferrell. S. Liu, C.S. Kuo, and J. Long assembled the hormone list. M.F.Z. Wang and I.D. Vlaminck performed uTAR analysis on the candidate lemur LHB gene. S. Wang calculated the cell ontology distances. S. Liu, J. Epelbaum, and J. Terrien analyzed the seasonally oscillating hormones. S. Liu and C.S. Kuo performed the RNAscope experiments. K. Awayan constructed the interactive web portal. The Tabula *Microcebus* Consortium constructed the mouse lemur molecular cell atlas. S. Liu and J.E. Ferrell wrote the manuscript with input from all authors.

Competing interests

The authors declare no competing interests.

Additional information

Supplementary information The online version contains supplementary material available at <https://doi.org/10.1038/s41467-024-46070-9>.

Correspondence and requests for materials should be addressed to ? Mark A. Krasnow? or James E. Ferrell Jr.

Peer review information *Nature Communications* thanks Anna Wilbrey-Clark and the other anonymous reviewers for their contribution to the peer review of this work.

Reprints and permissions information is available at <http://www.nature.com/reprints>

Publisher's note Springer Nature remains neutral with regard to jurisdictional claims in published maps and institutional affiliations.

Open Access This article is licensed under a Creative Commons Attribution 4.0 International License, which permits use, sharing, adaptation, distribution and reproduction in any medium or format, as long as you give appropriate credit to the original author(s) and the source, provide a link to the Creative Commons licence, and indicate if changes were made. The images or other third party material in this article are included in the article's Creative Commons licence, unless indicated otherwise in a credit line to the material. If material is not included in the article's Creative Commons licence and your intended use is not permitted by statutory regulation or exceeds the permitted use, you will need to obtain permission directly from the copyright holder. To view a copy of this licence, visit <http://creativecommons.org/licenses/by/4.0/>.

© The Author(s) 2024

The Tabula Microcebus Consortium

Shixuan Liu^{1,2,3}, Camille Ezran^{2,3}, Michael F. Z. Wang⁴, Zhengda Li¹, Kyle Awayan⁵, Jonathan Z. Long^{6,7}, Iwijn De Vlaminck⁴, Sheng Wang⁸, Jacques Epelbaum⁹, Christin S. Kuo¹⁰, Jérémy Terrien⁹, Mark A. Krasnow^{2,3}, James E. Ferrell Jr.^{1,2}, Snigdha Agarwal⁵, Aditi Agrawal⁵, Ahmad Al-Moujahed¹¹, Alina Alam¹², Megan A. Albertelli¹³, Paul Allegakoen¹⁴, Thomas Ambrosi¹², Jane Antony¹², Steven Artandi^{2,15,16}, Fabienne Aujard⁹, Ankit Baghel¹⁷, Isaac Bakerman¹⁸, Trygve. E. Bakken¹⁹, Jalal Baruni^{2,3,17,20}, Philip Beachy^{1,12,21,22}, Biter Bilen²³, Olga Botvinnik⁵, Scott. D. Boyd⁶, Deviana Burhan²⁴, Kerriann M. Casey¹³, Charles Chan¹², Charles. A. Chang^{21,25}, Stephen Chang^{2,3,18}, Ming Chen²⁶, Michael F. Clarke¹², Sheela Crasta⁵, Rebecca Culver²⁶, Jessica D'Addabbo^{27,28}, Spyros Darmanis⁵, Roozbeh Dehghannasiri^{2,29}, Song-Lin Ding¹⁹, Connor V. Duffy^{3,26}, F. Hernán Espinoza^{2,3}, Jean Farup^{23,30}, Hannah K. Frank^{6,31}, Margaret Fuller^{21,26}, Astrid Gillich^{2,3}, Elias Godoy¹³, Dita Gratzinger⁶, Lisbeth A. Guethlein^{32,33}, Yan Hang^{21,25}, Kazuteru Hasegawa^{2,15,16}, Rebecca D. Hodge¹⁹, Malachia Hoover¹², Franklin W. Huang¹⁴, Kerwyn C. Huang^{5,33,34}, Shelly Huynh⁵, Taichi Isobe³⁵, Carly Israel⁵, SoRi Jang^{2,3}, Qiuyu Jing³⁶, Robert C. Jones³⁴, Jengmin Kang²³, Caitlin J. Karanewsky^{2,3}, Jim Karknias⁵, Justus Kebschull³⁷, Aaron Kershner^{2,38}, Lily Kim²⁶, Seung K. Kim^{16,21,25,39}, E. Christopher Kirk⁴⁰, Winston Koh^{41,42}, Silvana Konermann^{2,3}, William Kong¹², Corinne Lautier⁴³, Song Eun Lee^{23,44}, Ed S. Lein¹⁹, Rebecca Lewis⁴⁰, Peng Li^{2,3}, Shengda Lin⁴⁵, Yin Liu^{2,3}, Gabriel Loeb⁴⁶, Wan-Jin Lu¹², Katherine Lucot⁶, Liqun Luo^{3,17}, Ashley Maynard⁵, Aaron McGeever⁵, Ross Metzger^{10,47}, Jingsi Ming^{48,49}, Tom Montine⁶, Antoine de Morree^{23,30}, Maurizio Morri⁵, Karim Mrouj¹², Shravani Mukherjee¹¹, Ahmad Nabhan^{2,3}, Saba Nafees⁵, Norma Neff⁵, Patrick Neuhöfer^{2,15,16}, Patricia Nguyen^{16,27,28}, Jennifer Okamoto⁵, Julia Olivier⁵⁰, Youcef Ouadah^{2,51}, Honor Paine²⁴, Peter Parham^{32,33}, Jozeph L. Pendleton^{2,3}, Lolita Penland⁵, Martine Perret⁹, Angela Oliveira Pisco⁵, Zhen Qi¹², Stephen R. Quake^{5,34,52}, Ute Radespiel⁵³, Thomas A. Rando²³, Hajaririna Noëline Ravelonjanahary⁵⁴, Andriamahery Razafindrakoto⁵⁴, Julia Salzman^{2,29}, Nicholas Schaum²³, Robert Schopler⁵⁵, Bronwyn Scott¹¹, Liza Shapiro⁴⁰, Hosu Sin²¹, Rahul Sinha⁵⁶, Rene Sit⁵, Geoff Stanley³⁴, Lubert Stryer⁵⁷, Varun Ramanan Subramaniam¹¹, Aditi Swarup¹¹, Michelle Tan⁵, Weilun Tan⁵, Alexander Tarashansky^{5,34}, Aris Taychameekiatchai²⁴, Kyle J. Travaglini^{2,3}, Andoni Urtasun²³, Sivakamasundari V¹², Avin Veerakumar^{2,3,34,58}, Venkata N. P. Vemuri⁵, Jean-Michel Verdier⁴³, Douglas Vollrath²⁶, Bo Wang³⁴, Bruce Wang²⁴, Gefei Wang⁴⁹, James Webber⁵, Hannah Weinstein^{14,59,60}, Irving L. Weissman⁵⁶, Amanda L. Wiggenhorn^{6,61}, Cathy V. Williams⁵⁵, Patricia Wright⁶², Albert Y. Wu¹¹, Angela Ruohao Wu^{36,63,64}, Timothy Ting-Hsuan Wu^{2,3}, Tony Wyss-Coray^{23,44}, BaoXiang Li¹¹, Jia Yan⁵, Can Yang⁴⁹, Jinxurong Yang³⁶, Anne D. Yoder⁶⁵, Brian Yu⁵, Andrea R. Yung^{2,3}, Yue Zhang^{3,17}, Jia Zhao⁴⁹ & Zicheng Zhao^{3,13}

¹¹Department of Ophthalmology, Stanford University School of Medicine, Stanford, CA, USA. ¹²Institute for Stem Cell Biology and Regenerative Medicine, Stanford University School of Medicine, Stanford, CA, USA. ¹³Department of Comparative Medicine, Stanford University School of Medicine, Stanford, CA, USA. ¹⁴Division of Hematology/Oncology, Department of Medicine, University of California San Francisco, San Francisco, CA, USA. ¹⁵Stanford Cancer Institute, Stanford University School of Medicine, Stanford, CA, USA. ¹⁶Department of Medicine, Stanford University School of Medicine, Stanford, CA, USA. ¹⁷Department of Biology, Stanford University, Stanford, CA, USA. ¹⁸Department of Medicine, Division of Cardiovascular Medicine, Stanford University, Stanford, CA, USA. ¹⁹Human Cell Types Department, Allen Institute for Brain Science, Seattle, WA, USA. ²⁰Department of Anesthesiology, Perioperative and

Pain Medicine, Stanford University School of Medicine, Stanford, CA, USA. ²¹Department of Developmental Biology, Stanford University School of Medicine, Stanford, CA, USA. ²²Department of Urology, Stanford University School of Medicine, Stanford, CA, USA. ²³Department of Neurology and Neurological Sciences, Stanford University School of Medicine, Stanford, CA, USA. ²⁴Department of Medicine and Liver Center, University of California San Francisco, San Francisco, CA, USA. ²⁵Stanford Diabetes Research Center, Stanford, CA, USA. ²⁶Department of Genetics, Stanford University School of Medicine, Stanford, CA, USA. ²⁷Division of Cardiovascular Medicine, Stanford University, Stanford, CA, USA. ²⁸Stanford Cardiovascular Institute, Stanford, CA, USA. ²⁹Department of Biomedical Data Science, Stanford University, Stanford, CA, USA. ³⁰Department of Biomedicine, Aarhus University, Aarhus, Denmark. ³¹Department of Ecology and Evolutionary Biology, Tulane University, New Orleans, LA, USA. ³²Department of Structural Biology, Stanford University School of Medicine, Stanford, CA, USA. ³³Department of Microbiology and Immunology, Stanford University School of Medicine, Stanford, CA, USA. ³⁴Department of Bioengineering, Stanford University, Stanford, CA, USA. ³⁵Department of Oncology and Social Medicine, Kyushu University, Fukuoka, Japan. ³⁶Division of Life Science, Hong Kong University of Science and Technology, Hong Kong SAR, China. ³⁷Department of Biomedical Engineering, Johns Hopkins School of Medicine, Baltimore, MD, USA. ³⁸Institute of Stem Cell Biology and Regenerative Medicine, Stanford University School of Medicine, Stanford, CA, USA. ³⁹JDRF Center of Excellence, Stanford, CA, USA. ⁴⁰Department of Anthropology, University of Texas at Austin, Austin, TX, USA. ⁴¹Institute of Bioengineering and Bioimaging, Agency of Science Technology and Research, Singapore, Singapore. ⁴²Bioinformatics Institute, Agency of Science Technology and Research, Singapore, Singapore. ⁴³MMDN, University of Montpellier, EPHE-PSL, INSERM, Montpellier, France. ⁴⁴Wu Tsai Neurosciences Institute, Stanford, CA, USA. ⁴⁵Zhejiang Provincial Key Laboratory for Cancer Molecular Cell Biology, Life Sciences Institute, Zhejiang University, Hangzhou, Zhejiang, China. ⁴⁶Division of Nephrology, Department of Medicine, University of California San Francisco, San Francisco, CA, USA. ⁴⁷Division of Cardiology, Stanford University School of Medicine, Stanford, CA, USA. ⁴⁸Academy of Statistics and Interdisciplinary Sciences, KLATASDS-MOE, East China Normal University, Shanghai, China. ⁴⁹Department of Mathematics, Hong Kong University of Science and Technology, Hong Kong, SAR, China. ⁵⁰Institute for Computational and Mathematical Engineering, Stanford University, Stanford, CA, USA. ⁵¹Program in Cancer Biology, Stanford University School of Medicine, Stanford, CA, USA. ⁵²Department of Applied Physics, Stanford University, Stanford, CA, USA. ⁵³Institute of Zoology, University of Veterinary Medicine Hannover, Hannover, Germany. ⁵⁴Department of Animal Biology, Faculty of Science, University of Antananarivo, Antananarivo 101, BP 566, Madagascar. ⁵⁵Duke Lemur Center, Durham, NC, USA. ⁵⁶Stanford Institute for Stem Cell Biology and Regenerative Medicine, Stanford, CA, USA. ⁵⁷Department of Neurobiology, Stanford University School of Medicine, Stanford, CA, USA. ⁵⁸Medical Scientist Training Program, Stanford University School of Medicine, Stanford, CA, USA. ⁵⁹Helen Diller Family Comprehensive Cancer Center, University of California San Francisco, San Francisco, CA, USA. ⁶⁰Bakar Computational Health Sciences Institute, University of California San Francisco, San Francisco, CA, USA. ⁶¹Department of Chemistry, Stanford University, Stanford, CA, USA. ⁶²Department of Anthropology, Stony Brook University, Stony Brook, NY, USA. ⁶³Department of Chemical and Biological Engineering, Hong Kong University of Science and Technology, Hong Kong SAR, China. ⁶⁴Center for Aging Science, Hong Kong University of Science and Technology, Hong Kong, SAR, China. ⁶⁵Department of Biology, University Program in Genetics & Genomics, Duke University, Durham, NC, USA.